HHS Public Access

Author manuscript

J Physiol. Author manuscript; available in PMC 2021 February 01.

Published in final edited form as:

J Physiol. 2020 February ; 598(4): 853–889. doi:10.1113/JP278680.

Synaptic cleft microenvironment influences potassium permeation and synaptic transmission in hair cells surrounded by calyx afferents in the turtle

Donatella Contini[1], **Gay R. Holstein**[2], **Jonathan J. Art**[1]

[1]Department of Anatomy & Cell Biology, University of Illinois College of Medicine, 808 S. Wood St, Chicago, IL 60612, USA.

[2]Neurology, Icahn School of Medicine at Mount Sinai, 1468 Madison Ave, New York, NY 10029

Abstract

In the vertebrate nervous system, ions accumulate in diffusion-limited synaptic clefts during ongoing activity. Such accumulation can be demonstrated at large appositions such as the hair cell – calyx afferent synapses present in central regions of the turtle vestibular semicircular canal epithelia. Type I hair cells influence discharge rates in their calyx afferents by modulating the potassium concentration in the synaptic cleft, $[K^+]_c$, which regulates potassium-sensitive conductances in both hair cell and afferent. Dual recordings from synaptic pairs have demonstrated that, despite a decreased driving force due to potassium accumulation, hair cell depolarization elicits sustained outward currents in the hair cell, and a maintained inward current in the afferent. We used kinetic and pharmacological dissection of the hair cell conductances to understand the interdependence of channel gating and permeation in the context of such restricted extracellular spaces. Hair cell depolarization leads to calcium influx and activation of a large calcium-activated potassium conductance, G_{BK}, that can be blocked by agents that disrupt calcium influx or buffer the elevation of $[Ca^{2+}]_i$, as well as by the specific $K_{Ca}1.1$ blocker Iberiotoxin. Efflux of K^+ through G_{BK} can rapidly elevate $[K^+]_c$, which speeds the activation and slows the inactivation and deactivation of a second potassium conductance, $G_{K(LV)}$. Elevation of $[K^+]_c$ or chelation of $[Ca^{2+}]_c$ linearizes the $G_{K(LV)}$ steady-state I–V curve, consistent with a K^+-dependent relief of Ca^{2+}-inactivation of $G_{K(LV)}$. As a result, this potassium-sensitive hair cell conductance pairs with the potassium-sensitive HCN conductance in the afferent and creates resistive coupling at the synaptic cleft.

Correspondence: jart@uic.edu.

Author contributions

D.C. was involved in the conception, design, collection and analysis of data, and drafting the manuscript. G.R.H. was involved in the conception, design, interpretation of the data, and drafting the manuscript. J.J.A. contributed to the conception, design, collection, assembly, data analysis, interpretation, and drafting the manuscript.

Additional Information

The authors have no competing or conflicts of interest.

Introduction:

Ongoing neural activity is associated with rapid and dynamic changes in ion concentration at many synaptic sites in the brain, especially at those enveloped by astrocytic processes (Špaček, 1985; Ventura & Harris, 1999). These changes are not reflected in the bulk extracellular solution, and measuring them poses technical challenges (Larsen *et al.*, 2019) given the minute volumes and the speed with which ions diffuse and concentrations vary. There are locations within the central auditory and peripheral vestibular systems, however, where calyces (Retzius, 1884; Held, 1893) form large appositions between presynaptic and postsynaptic cells, and where the dynamics of synaptic transmission and ion accumulation can be measured using electrophysiological (Forsythe, 1994; Lim *et al.*, 2011; Contini *et al.*, 2012; Contini *et al.*, 2017) or optical (Highstein *et al.*, 2014) techniques. It is clear from those studies that depolarization and vesicular fusion during synaptic transmission can lead not only to the accumulation of K^+, but also to elevation of $[H^+]_c$ within the synaptic cleft. Accumulation of the latter (DeVries, 2001; Cho & von Gersdorff, 2014) might reduce the hair cell L-type calcium current, $I_{CaV1.3}$, (Zidanic & Fuchs, 1995; Green *et al.*, 1996; Schnee & Ricci, 2003) necessary for quantal transmission, and accumulation of either H^+ or K^+ could have modulatory effects on conductances responsible for elevating $[K^+]_c$ (Steidl & Yool, 1999; Contini *et al.*, 2012; Contini *et al.*, 2017). In particular, the potassium-sensitive change in the kinetics of the potassium current in type I hair cells enveloped by a calyx afferent suggests that, in addition to any inherent voltage-sensitivity it may have, the kinetics of the conductance activation and inactivation has a sensitivity to $[K^+]_c$ as well. In fact, this has been observed in squid axon (Swenson & Armstrong, 1981) and other K_V1 and K_V2 channels (Baukrowitz & Yellen, 1995; Levy & Deutsch, 1996).

While it is clear how changes in potassium concentration might affect conductance or shift the equilibrium potential, it is not yet clear how such a potassium-sensitive change in kinetics would be imparted to the potassium conductances previously described in vestibular hair cells (Rennie & Correia, 1994; Rusch & Eatock, 1996; Rennie & Correia, 2000; Brichta *et al.*, 2002). Moreover, it is not obvious if, and to what extent, potassium flux through one channel might affect permeation through other channels enveloped by the same afferent ending. As a result, the restricted volume of the synaptic cleft defines an ionic environment that cannot easily be replicated using solitary cells because bulk solutions fail to mimic the likely dynamic changes occurring *in situ*. As a consequence, the functional significance of the ionic interactions within the confines of a synapse, as well as the regulation of permeation through each of the conductances, remains obscure.

Permeation through an ion channel pore can be regulated by allosteric effects due to mechanical and electrical forces as well as chemical binding. The process is often complex, and channels such as the large, calcium-activated potassium channel, $K_{Ca}1.1$, is gated by both internal Ca^{2+} and voltage (Marty, 1981; Latorre *et al.*, 1982), and inhibited at positive potentials by $[H^+]_i$ (Brelidze & Magleby, 2004), $[Ca^{2+}]_i$ and $[Mg^{2+}]_i$ (Geng *et al.*, 2013). More generally, there is mounting evidence that, in addition to any voltage- or ligand-dependent gating a particular channel may have, permeation is affected by secondary monovalent or divalent binding (Nelson, 1986; Mayer & Westbrook, 1987; Immke & McCleskey, 2003), internal occlusion by N-terminal amino acids (Armstrong & Bezanilla,

1977; Zagotta *et al.*, 1990) and/or by external ionic binding that affects the selectivity filter (Grissmer & Cahalan, 1989; Cuello *et al.*, 2010). This is true for members of the sodium (Woodhull, 1973; Sun *et al.*, 1997), potassium (Gomez-Lagunas *et al.*, 2003; Carrillo *et al.*, 2015), and cyclic-nucleotide-gated channel families (Haynes *et al.*, 1986; Root & MacKinnon, 1994). In fact, for many of these, the kinetics and amplitude of their currents can be explicitly modulated by manipulation of $[H^+]_o$, $[Ca^{2+}]_o$, or $[K^+]_o$ (Zhang & Siegelbaum, 1991; Gomez-Lagunas *et al.*, 2003; Contini *et al.*, 2012).

The effect of blocking permeation as a means of imparting voltage sensitivity has been examined in anomalous or inward rectification (Armstrong, 1969) and modeled in the H^+ and Ca^{2+} block of the skeletal muscle Na^+ conductance (Woodhull, 1973). For inward rectification, ions (Horie *et al.*, 1987; Matsuda *et al.*, 1987) or peptides (Lopatin *et al.*, 1994) can impart a direction-dependent block of the channel. The detailed shape of these curves is consistent with a range of affinities at sites within the pore that prevent outward current in a voltage-dependent manner. The analogous question of whether such a process might also occur for outwardly rectifying conductances has not been addressed substantially. In principle, outward rectification could obtain if the selectivity filter is altered by nearby voltage-dependent allosteric binding that is relieved by depolarization (Panaghie *et al.*, 2008; Hoshi & Armstrong, 2013; Kratochvil *et al.*, 2017). This might be a direct effect, or could occur through an interaction with ions whose external concentration increases following depolarization and ion accumulation in a diffusion-limited extracellular space.

To address these issues, we have exploited kinetic and pharmacological differences to isolate the conductances activated with depolarization in vestibular hair cells surrounded by calyx afferents. We wished to determine the extent to which currents are dependent, in part, on prior activation of other conductances and ion flux into the restricted synaptic cleft. Our results are consistent with the activation of a rapid inward calcium current, followed by a calcium-activated potassium conductance. The associated potassium flux into the cleft serves to speed the activation of a second, slower, potassium conductance. The permeation through the latter is modulated by a potassium-sensitive relief of inactivation. As a result, this potassium-sensitive hair cell conductance may pair with the potassium-sensitive HCN conductance in the afferent and create resistive coupling of the two at the synaptic cleft.

Methods:

Ethical Approval

Experiments used tissue harvested from red–eared turtles, *Trachemys scripta elegans*, housed in the AAALAC accredited, UIC Biologic Resources Laboratory. Experimental protocols were approved by the University of Illinois at Chicago Animal Care and Use Committee, according to National Institutes of Health guidelines (assurance number A3460–01). Turtles were killed, and decapitated following IM injection of Ketamine, 6 mg/kg, according to the American Veterinary Medical Association guidelines.

Epithelia isolation

The details of the tissue preparation and isolation have been given previously (Contini *et al.*, 2017). Briefly, all experiments were performed on isolated vestibular epithelia from the posterior semicircular canal of turtles of either sex (carapace 9 – 15 cm, 132 – 140g, n = 93, 54 males, 39 females). Following decapitation, the head was split in the mid-sagittal plane and immersed in a 4˚C, oxygenated low-Ca^+ Ringer's containing (in mM), 121 NaCl, 4 KCl, 0.45 $CaCl_2$, 2.2 $MgCl_2$, 10 Na-HEPES, 2 Na-Pyruvate, 2 Creatine monohydrate, at pH 7.6. The posterior canal epithelium was dissected free, and hair cells and enveloping afferent terminals were visualized from the lateral aspect by bisecting the epithelium along the ridge of the crista normal to the axis of the canal, and removing the upper side of the epithelium.

Microscopic visualization, salt solutions, and reconstruction

As in prior experiments (Contini *et al.*, 2017), 320 μl experimental chambers were mounted on a fixed-stage, upright, Zeiss Axioskop FS-II microscope, and perfused at 1 ml/min with 24 – 27˚C oxygenated artificial perilymph (in mM), 121 NaCl, 4 KCl, 2.8 $CaCl_2$, 2.2 $MgCl_2$, 10 Na-HEPES, 2 Na-Pyruvate, 2 Creatine monohydrate, at pH 7.6. Physiological salts were purchased primarily from Sigma-Aldrich, (RRID:SCR_008988) and Fisher BioReagents, (RRID:SCR_003374). Exceptions included more exotic toxins, blockers and buffers including Iberiotoxin, IbTX, (Tocris Bioscience, Batch #14A, #24A, RRID:SCR_003689); Compound VIII (EMD Millipore Corporation, San Billerica, MA, USA, Lot #D00147760 – no longer commercially available); and BAPTA-4K (Molecular Probes RRID:SCR_013318).

The epithelia were visualized using a Zeiss 40X, 0.8 NA, 3.6 mm working distance water immersion objective, with additional 2X optovar magnification. Both video low-light Differential Interference Contrast (DIC) and widefield fluorescence images were captured using an $iXon_3$ 897, EMCCD camera, QE > 90% (Andor Technology, Belfast, UK). For confocal verification of the hair cell – afferent couplet, the tissue was prepared as before (Contini *et al.*, 2017), image stacks were acquired using a LSM 710 Confocal Microscope (Zeiss, Thornwood, NY, USA), and digitally reconstructed (ZEN Digital Imaging for Light Microscopy, RRID:SCR_013672).

Electrophysiology

Dual-electrode recordings from hair cell – afferent couplets were made with borosilicate electrodes (World Precision Instruments, Cat# 1B150F-4 RRID:SCR_008593). The afferent electrodes were filled with (in mM): 118 KF, 12 KCl, 5 K_2-EGTA, 5.45 K-HEPES, 5 Na_2ATP, 175 μM Li_2-GTP, at pH 7.2. Except where noted, the corresponding hair cell electrodes were filled with: 115 KCl, 5.3 $MgCl_2$, 0.45 $CaCl_2$, 5 K_2-EGTA, 10 K-HEPES, 5 Na_2ATP, 5 Creatine Phosphate, at pH 7.2. To facilitate reconstruction of confocal image stacks, 50 μM Alexa Fluor 568 was added to the afferent electrodes, and 50 μM Alexa Fluor 488 to the hair cell electrodes (Molecular Probes, RRID:SCR_013318). Simultaneous presynaptic and postsynaptic recordings were made with a MultiClamp 700B amplifier (Molecular Devices, Sunnyvale, CA, USA). Electrode capacitance and liquid junction potentials (average −53 mV for KF/KCl-based electrodes, and −4 mV for KCl electrodes) were offset just prior to sealing onto the cells.

Recording electrodes had initial series resistances in the bath of 3 – 5 MΩ, and final resistances upon achieving whole-cell configuration of ~3*X* their initial values. The amplifier compensation circuit was used to compensate up to 65% of the access resistance, when compensatory feedback was low-pass filtered at 4.5 – 5.0 kHz. This resulted in final access resistances close to the initial values measured in the bath. We used the capacity transients at the beginning and the end of small, ± 10 mV, voltage commands from −100 mV embedded in the voltage-clamp protocols to estimate the access resistance, membrane resistance, and whole-cell capacitance of both cells. Since the capacity transient was used to monitor changes in access resistance continuously during the experiments, only the R_s 'correction' circuit on the amplifier was used, and the 'prediction' circuit was set to zero. The access resistance, R_a, the sum of the pipette series resistance and the resistance through the synaptic cleft to the bath, was determined from the current necessary to charge the membrane and the time constant, τ, of the current relaxation to I_∞, where $\tau = C_m R_{(Ra||Rm)}$. Details of the analysis were given previously (Contini *et al.*, 2017).

Though stimuli are given as command voltages, all figures derived from current measurements: conductance-voltage (G-V), I-V curves, and reversal potential - versus voltage, were corrected for voltage drops due to the average current flow across uncompensated access resistance over the interval of the command potential being measured. Voltage commands of 25 ms were given at 200 ms intervals except where dictated by the time to reach steady-state, or to return to the baseline current at a holding potential. Whole-cell currents were typically converted using a 50 MΩ feedback resistor for the hair cell, and 500 MΩ resistor for the afferent fiber. Currents and voltages were low-pass filtered at 10 kHz using 4-pole Bessel filters, and digitized at 200 kHz. All digitization, as well as voltage and current commands, were under the control of a Digidata 1440A interface (Molecular Devices, Sunnyvale, CA, USA).

Drug Perfusion

Rapid, local solution exchange was achieved by positioning the output of a Teflon MPP6 manifold (Warner Instruments, Hamden, CT USA) within 100 μm of the cell pair. For most experiments, the barrels of the manifold were supplied by a recirculating Rainin Rabbit peristaltic pump (Gilson, Middleton, WI, USA), with the solution of choice directed to the manifold using a remote-controlled miniature solenoid valve (The Lee Co., Westbrook, CT, USA). For experiments using IbTX the manifold was supplied by a DAD – VM 9-channel pressurized perfusion system (ALA Scientific Instruments, Farmingdale, NY, USA) to minimize peptide loss through adhesion to the plastic tubing. Initial effects of perfusion could be recorded within six seconds of the onset of superfusion, and efficient washout was assured by having normal perilymph in at least one of the manifold barrels, in addition to the bath perfusion.

Statistics & Curve fitting

Stimulus protocols and digitization were under software control (Molecular Devices, pClamp v10, RRID:SCR_011323). Data were imported using IGOR-compatible routines (Rothman & Silver, 2018) (NeuroMatic v3_0c RRID:SCR_004186). Off-line signal

processing, analysis, and figure creation used technical graphing and data analysis software (IGOR Pro, v8, RRID:SCR_000325).

The statistics of current and voltage records were calculated in the usual way for equally-spaced data: average of all Y_i values, a; standard deviation, σ, of n values, $\sigma = \sqrt{1/(n-1)\sum (Y_i - a)^2}$; root-mean-square of Y_i, $rms = \sqrt{(1/n)\sum Y_i^2}$. Where noted, some current traces were Gaussian filtered using binomial smoothing functions (Marchand & Marmet, 1983) within IGOR Pro. With 200 kHz digitization, the underlying filters typically had half-power 3_{dB} amplitudes at 4328 Hz. The half-amplitude frequency was given by:

$f_{1/2} = (2/\pi)\, cos^{-1} 0.5^{1/2n}$, where n is the number of filter iterations.

Non-linear fits to all functions were solved by an iterative least-squares method modeled on the code in Numerical Recipes in C, (Press *et al.*, 1992). Where appropriate, estimates of the errors in the fit coefficients are given. They are computed from a linearized quadratic approximation to the chi-square surface at the solution. The current waveform of exponential decay of capacity transients and leakage currents at −100 mV were fit with either exponential or double exponential functions with offset, $I_0 + I_1 e^{(t-t_0)/\tau}$, $I_o + I_1 e^{(t-t_0)/\tau_1} + I_2 e^{(t-t_0)/\tau_2}$, where y_0 was the minimum value, I_1 and I_2 were amplitudes, and τ_1 and τ_2 were time constants. In the current traces illustrated in results, scaled versions of these fits were subtracted from the raw current traces over the pulse interval to eliminate the capacity transients and leakage to 0 mV. With the exception of the results in Fig. 9, the current at the holding potential was corrected for the leakage current as well. The total current elicited by depolarization under different experimental conditions was fit to exponential recovery functions of the form,

$$I_{Total} = \sum_{i=0}^{3} I_i \bullet \left(1 - \exp\left(\frac{-t + t_i}{\tau_{(V)i}}\right)\right)^{n_i}, \quad (1)$$

where the I_i were the amplitudes, the t_i were the time of onset of response to the step, the $\tau_{(V)i}$ were the voltage-dependent time constants for each current, and the n_i were integral powers that gave the best fit to the onset of the component currents. The equation is given in expanded form for a leak current, I_0, and the three voltage-activated currents, $I_{1,2,3}$ in Eq. 5 in Results. To account for the slowing of instantaneous currents through conductances on at the holding potential, an additional term was added representing the time constant of the recording system.

The conductance vs voltage curves were fit with sigmoidal functions of the form,

$$g(V) = g_0 + \left(\frac{g_\infty}{\left(1 + e^{-\frac{(V - V_{0.5})}{k}} \right)} \right), \quad (2)$$

where the free parameters, g_0 and g_∞ were the limiting conductances, $V_{0.5}$ the voltage of half activation, and k, the slope at half activation.

Results:

Kinetic separation of currents activated by depolarization.

Consistent with prior experiments using long, 500 ms, depolarizations (Contini *et al.*, 2017), 25 ms voltage steps elicited an initial rapid inward current followed by progressively larger outward current (Fig. 1A, middle panel and inset). Outward currents in the hair cell were associated with corresponding inward currents in the afferent calyx (Fig. 1A, bottom panel), the largest of which activated TTX-blockable currents that likely represent initiation of action potentials (APs) at a spike initiation zone located more proximal to the CNS than the afferent recording electrode and not under voltage clamp (Contini *et al.*, 2017).

To separate conductances by their activation kinetics, hair cells were held at −100 mV, a potential at which many channels that open upon depolarization occupy a closed state furthest from a closed-to-open transition. With the potential of the enveloping afferent held constant at −100 mV, the hair cell was depolarized to potentials between −70 and 90 mV (Fig. 1A, top panel). The complexity of the temporal sequence of current activation was visible in the first five milliseconds of the step response (Fig. 1A, middle panel inset). With depolarizations above −50 mV, an inward current activated rapidly, and increased in amplitude, reaching a peak of −320 pA (−192.3 ± 84.3 pA, mean ± S.D., n = 9) for a −20 mV command. A simple and precise measurement of an I-V for the initial component was precluded by the activation of outward current that increased in amplitude and speed with increased depolarization. This outward current had two phases, an initial rapid outward phase that for small depolarizations above −50 mV reached a discernable plateau, and a second slowly rising phase that began progressively earlier for larger depolarizations. In principle, this behavior in the outward current might represent either two modes of channel gating (Blatz & Magleby, 1986; McManus & Magleby, 1988; Cruz-Rangel *et al.*, 2015), or the existence of two kinetically different channels. The latter was considered more likely since the later slow outward current could be observed at more hyperpolarized potentials in the absence of the early fast outward one.

Current activation was observed in more detail between −60 and −40 mV (Fig. 1B). The slower outward current was first discernable from noise at −60 mV, and grew to a maximum of 71 pA by the end of the 25 ms pulse. At −50 mV, −35 pA of rapid inward current could be measured, followed by 32 pA of rapid outward component, to which 404 pA of slow

outward current was added by the end of the pulse. At −40 mV, all three hair cell currents were robust, reaching peaks of −108, 305, and 797 pA, respectively. The induced afferent current was correlated with increases in both components of the outward current (Fig. 1B, bottom panel). Occasional EPSCs were observed (Fig. 1B, bottom panel, arrow) that had half-widths more than one S.D. wider than the mean of EPSCs elicited by depolarizations of the hair cell, perhaps reflecting synaptic input from the centrifugal efferent system since the VIIIth nerve and brainstem remained attached to our preparation.

Isochronal I-V measurements for the initial (open circles) and final (filled-circles) outward currents (Fig. 1C) demonstrated that the slow component activated at more hyperpolarized potentials, and both fast and slow outward currents were activated at potentials depolarized above −50 mV. The ratio of the two components was non-monotonic, reaching a maximum of 2.77 near 0 mV (2.28 ± 0.77, n = 10), at which point the two curves began to converge. This convergence was likely the result of the second component activating rapidly enough to be increasingly included in the early isochronal measurement. Repolarization of the hair cell to −100 mV elicited large, slowly decaying inward currents. The slope of the chord connecting the outward current at the end of the pulse to the peak of the inward current upon repolarization (Fig. 1C) was used as a measure of the conductance at the end of the pulse, as illustrated for three pairs (a, b, and c). Normalized activation curves for 11 cells are shown (Fig. 1D) together with a scatter plot of the maximum conductance (Fig. 1D, inset). The zero-current crossing of the chord (Fig. 1C) could, in turn, be used to estimate the voltage-dependence of the equilibrium potential for the conductance at the moment of transition back to the holding potential (Fig. 1E). After 25 ms of depolarization, there was an average rightward shift in the equilibrium potential at rates of 1.01 – 5.56 mV per 10 mV of hair cell depolarization for potentials between −70 and −40 mV. These rates decreased to 0.22 – 0.68 mV shift in E_K per 10 mV, on average, for depolarizations above −30 mV. This suggests that even with brief depolarizations, the $[K^+]_c$ elevates rapidly with initial depolarization, and then slows at more depolarized potentials to values that yield the average rate of ~4 mV estimated previously from prolonged, 500 ms, pulses (Contini *et al.*, 2017).

Following substitution of Na^+ for K^+, and the addition of 20 mM 4-Aminopyridinium (4-AP$^+$) and 30 mM Tetraethylammonium-Chloride (TEA-Cl) in the hair cell pipette solution, the outward hair cell current was blocked, and the development of an additional inward current in the afferent was suppressed (data not shown). These results are consistent with our prior demonstration that outward potassium current from the hair cell is necessary and sufficient to rapidly elevate the potassium concentration in the cleft, $[K^+]_o$, and depolarize the potassium equilibrium potential (Contini *et al.*, 2017). It remained to be determined whether the complex time course of the outward potassium current represented different modes of gating of a single conductance or a difference in kinetics of two conductances, and if the latter, whether one conductance was dependent upon the other.

4-Aminopyridium sensitivity of the fast and slow components of the outward current.

Based on discernable activation of the slower outward current at −60 mV, a voltage hyperpolarized to the activation of the more rapid component, we assumed that the two outward currents resulted from two distinct ion channels that could be dissected

pharmacologically. First, we isolated the slower, potentially downstream conductance. Potassium currents sensitive to 4-AP have been identified in both vestibular (Lewis & Hudspeth, 1983; Steinacker & Romero, 1991; Rennie & Correia, 1994) and auditory (Kros & Crawford, 1990; Goodman & Art, 1996b) hair cells. 4-AP creates a use and voltage-dependent intracellular block of the channel pore (Kirsch & Narahashi, 1983). To restrict the block to the presynaptic hair cell and spare the postsynaptic afferent calyx, a charged, membrane impermeant form, 4-aminopyridinium, 4-AP^+, was substituted for potassium on an equimolar basis in its pipette solution. Prior experiments used external 4-AP perfusion (Rennie & Correia, 1994; Rusch & Eatock, 1996) and could examine the effect of multiple concentrations on each hair cell. Since 4-AP blocks from the internal face of the channel, such experiments relied on its membrane permeability to achieve the block. Under such circumstances, the rates of diffusion through the membrane and out to the recording pipette would determine the final internal concentrations, and as a result the precise half-blocking concentration was unknown. On the other hand, our experiments required normalizing to population data from multiple hair cells, each exposed to a single 4-AP^+ concentration, to generate the corresponding dose-response curves.

In these experiments, both the hair cell and afferent were held at −100 mV, and voltage commands to the hair cell ranged from −130 to 100 mV. Under control conditions in the absence of 4-AP^+, the outward currents during the last 5 ms of the 25 ms pulse were typically large, ranging from 2.81 to 16.87 nA (7.73 ± 4.37 nA, n = 14) (Fig. 2A) for a voltage command to 100 mV. The corresponding I-V curve, corrected for the voltage drop across the residual access resistance (Fig. 2A, inset), demonstrated that even with 65% compensation, the residual resistance prevented us from achieving the most depolarized potentials. However, the response changed dramatically upon inclusion of 150 μM 4-AP^+ (Fig. 2B). The decrease in the maximal current amplitude (Fig. 2B) typically resulted in lower voltage drops across the access resistance and an extended range of depolarization, as reflected in the I-V curve (Fig. 2B, inset). In addition to the significant reduction in total current, the fast component plateau was more apparent and the inflection between fast and slow components was more distinct (Fig. 2B, arrow and arrowhead). As seen in both the current traces and the corresponding I-V curve, the outward current decreased for depolarizations above 50 mV, a behavior reminiscent of the voltage-dependent block typically found in calcium-activated potassium conductances (Meech & Standen, 1975). The characteristics of the inward tail current produced upon repolarization changed with the inclusion of 4-AP^+ as well. In control experiments, the tail current had a complex time course (Fig. 2A), but with the addition of 150 μM 4-AP^+, the current could be well fit by the sum of two exponentials (Fig. 2B): a rapid one (2.12 ± 0.58 ms, n = 9) and a slower one (14.72 ± 6.41 ms) suggestive of the closing of two different conductances.

Increasing the blocker concentration by an order of magnitude to 1.5 mM 4-AP^+ (Fig. 2C) further reduced the total outward current. The early rapid component with its plateau was clearly visible, but the late slower component was vanishingly small, and the slow component in the tail current was >5% of control. The decrease in current at potentials greater than 50 mV was retained. An increase in concentration by another order of magnitude, to 15 mM 4-AP^+ (Fig. 2D), reduced the amplitude of the outward current even further. At this concentration, an additional inward component of the I-V curve was visible

between −50 and 0 mV. The traces of Fig. 2D are replicated in expanded view (Fig 2E), and it is apparent that the remaining outward current was superimposed on the rapid inward current (Fig. 2E, inset). Taken together, these results suggest that both the fast and slow components of the outward current were sensitive to 4-AP$^+$, but differed by more than an order of magnitude in their half-blocking dose, k_i. Taking the average early and late outward current amplitudes at each dose against the average current in the absence of 4-AP$^+$, the data could be fit (Fig. 2F) with a two-site inhibition binding curve,

$$I_K = I_o \bullet \left[A_f/\left(1+\left(K_f/x\right)^{n1}\right) + A_s/\left(1+\left(K_s/x\right)^{n2}\right)\right], \quad (3)$$

where I_o is the total potassium current at 0 mV in the absence of 4-AP$^+$, A_f and A_s are the relative amplitudes of fast and slow components, K_f and K_s are the 4-AP$^+$ concentrations required for half-block of each current, x is the 4-AP$^+$ concentration in the pipette, and n1, n2 are the respective coefficients of the two-component Hill function. The relative contributions, A_f and A_s, to the total current was set by their average 1:2.28 ratio based on the initial and final current amplitudes at 0 mV (Fig. 1B). From this, we estimate the half-blocking doses as 8.75 mM with a coefficient of 0.96 for the fast component and 233 μM with a coefficient of 0.93 for the slow component. We assume that in isolation these would correspond to single-site binding with coefficients of 1.0 for each of the two component currents. These values are similar, though larger than that for the slow current in vestibular hair cells (Rusch & Eatock, 1996), but comparable to 4-AP blocking of the fast and slow potassium currents in auditory hair cells in this species (Goodman & Art, 1996b).

This analysis also suggests that at the lowest concentration of 4-AP$^+$ used, 150 μM, the fast and slow components of the outward current were reduced to 98% and 60.1% of their control values, respectively. Since at this concentration there was little effect on the fast component, the ratio of fast to slow components under these conditions would be 1:1.36, which may explain why the kinetic differences between the two components were clearer under these conditions (Fig. 2B, arrow, arrowhead). Given the half-blocking doses for the fast and slow components when using the 15 mM concentration of 4-AP$^+$, we also expected that they would be reduced to 37% and 2% of their respective control values. This highlights the complexity of using pharmacological agents to estimate the contributions of multiple conductances that differ only in their half-blocking doses.

Sensitivity of the fast, outward current to Tetraethylammonium, TEA.

Based on these results, we estimated that the slower current would typically be reduced to ~2% by inclusion of 15 mM 4-AP$^+$ in the pipette, a maneuver that would allow us to examine the TEA sensitivity of the residual rapid outward current in isolation. Perfusing 6 mM TEA-Cl in the bath blocked a majority of the outward current and revealed that the rapidly activating inward current was maintained for the duration of the pulse (Fig. 3A, bottom). The amplitude of the current peaked between −50 and 0 mV as revealed in the associated steady-state I-V curve (Fig. 3A, inset). Prior studies in solitary auditory (Art & Fettiplace, 1987; Fuchs *et al.*, 1990) and vestibular (Lewis & Hudspeth, 1983; Ohmori, 1984) hair cells suggested that the time course of the current was consistent with a rapid inward calcium current followed by an outward potassium current.

In the absence of single-channel data, we applied a Hodgkin-Huxley formalism to the current remaining in 6 mM TEA-Cl. The onset of the currents could be modeled in the usual way as the sum of two exponential recovery functions raised to different powers,

$$I_{tot} = I_0 + I_{in} \bullet (1\text{-}\exp((-t+t_0)/\tau_{(v)0}))^{n0} + I_{out} \bullet (1\text{-}\exp((-t+t_0)/\tau_{(v)1}))^{n1}, \quad (4)$$

where I_{tot} was the total current, I_0 was the standing current at −100 mV, I_{in} and I_{out} were the amplitudes of the inward and outward currents, t_0 was the start of the pulse, $\tau_{(v)0}$ and $\tau_{(v)1}$ were the voltage-dependent time constants, and n_0 and n_1 were the corresponding powers of the currents.

Prior modeling differed as to the power that gave the best fit for the inward (Lewis & Hudspeth, 1983; Ohmori, 1984; Art & Fettiplace, 1987; Bao *et al.*, 2003) and outward (Hudspeth & Lewis, 1988; Art *et al.*, 1995) currents. Using integer values, we allowed n_0 to range between 1 and 3 and n_1 to range between 3 and 8, and calculated the least-square-error fit to the data for all combinations of n_0 and n_1. Of the 24 combinations, the best fit was achieved using $n_0 = 2$ and $n_1 = 6$. An expanded view of the current onset and its corresponding fit in the presence of 6 mM TEA-Cl (Fig. 3B) also suggested that the outward current was reduced to 9.4% of its control value. Assuming a single blocking site, this would correspond to a TEA half-blocking dose of 624 μM. To assess this, we constructed the I-V curves over a range of concentrations of TEA (Fig. 3C). For these curves, the shapes at each concentration are generally proportional and voltage-independent. Minor exceptions are at the highest doses where the inward current is revealed, and at the higher voltages, where the N-shaped block of residual outward current was less apparent. The aggregate data for the block of the potassium current at 0 mV versus concentration for 13 cells (Fig. 3D) was fit with a single-site inhibition binding curve. From this we estimate a half-blocking dose of 460 μM, a value 65% larger than that of the TEA block of the large, calcium-activated potassium conductance in turtle auditory hair cells (Goodman & Art, 1996b).

Internal BAPTA blocks the rapid and reduces the slow outward current.

To investigate the possible calcium dependence of the rapid component, we substituted 30 mM BAPTA-4K for the 5 mM EGTA in the recording pipette, with a compensatory reduction in potassium. Prior experiments in turtle auditory hair cells (Tucker & Fettiplace, 1996) and frog saccular hair cells (Roberts, 1993) suggested that the intrinsic calcium buffering is comparable to 1 mM BAPTA. In auditory and saccular hair cells, excess BAPTA blocked the electrical resonance by reducing the activation of the calcium-activated potassium conductance (Roberts, 1993). The three components in EGTA (Fig. 4A, middle panel), a rapid inward current followed by rapid and slow outward currents, reduced to a rapid inward current followed by only the slow outward current with 30 mM BAPTA in the pipette (Fig. 4A, bottom panel). The kinetic differences are highlighted by overlaying the two data sets in an expanded view of the first 4 ms (Fig. 4B). At each potential, the rapid inward current is followed by the rapid and slower outward components in EGTA-filled cells. In BAPTA-filled cells, the rapid outward current is eliminated, and the rapid inward current is followed after a delay by the slower outward current. Using the reasoning and

formalism of Eq. 4, we investigated adding a third term to represent I_{slow}, the slow outward current,

$$I_{tot} = I_0 + I_{in} \bullet (1-\exp((-t+t_0)/\tau_{(v)0}))^2 + I_{fast} \bullet (1-\exp((-t+t_0)/\tau_{(v)1}))^6 + I_{slow} \bullet (1-\exp((-t+t_1)/\tau_{(v)2}) \quad (5)$$

where, based on fits in the BAPTA experiments, the slow component was best represented by a delay followed by a single exponential function. The alternative Hodgkin-Huxley formalism required modeling the delay with extremely high powers, n > 25, which is unlikely to be realized biologically and is well outside the range of n-stage kinetic schemes typical of ion channels. Furthermore, a delay followed by simple exponential growth minimized the least-square-error in the fit of the model to the data during the initial rising phase. Based on 11 experiments using EGTA and 7 cells using BAPTA, we estimate from the fits that the second, rapid outward component is reduced to >1.01 % on average (S.D. = 0.171, n = 7) in BAPTA versus EGTA.

Two further differences in our fits to the EGTA and BAPTA results for voltage commands to −40 mV should be noted. Firstly, the delay in the onset of the slow outward current was shorter (t_1 = 2.95 ± 0.94 ms, n = 10) in EGTA than in BAPTA-filled cells (t_1 = 7.37 ± 1.12 ms, n = 7). Secondly, the time constant, $\tau_{(v)2}$, was faster for the EGTA-filled cells ($\tau_{(v)2}$ = 10.36 ± 7.28 ms) than for those filled with BAPTA ($\tau_{(v)2}$ = 17.46 ± 9.30 ms). The mean amplitude of the slow current at the end of the 25 ms pulse was less, but not significantly different at the p = 0.05 level between the two treatments. In agreement with data from Fig. 1B, a simple interpretation of the BAPTA experiments is that the initial rapid outward current was not obligatory for the activation of the slower outward current. However, the differences between EGTA and BAPTA results suggest that both the rapid and slow outward currents were calcium-sensitive, or that prior activation of the rapid outward current was able to augment the speed of activation of the second outward component.

Effects of a block of $Ca_V1.3$ on inward and outward currents.

Since increased calcium-buffering using an excess of BAPTA in the hair cell population systematically blocked the activation of the rapid outward current and increased the delay and time constant of the slow component, we next examined the calcium dependence in individual cells by blocking the hair cell $Ca_V1.3$ conductance (Zidanic & Fuchs, 1995; Green *et al.*, 1996; Schnee & Ricci, 2003) using the $Ca_V1.2/Ca_V1.3$ antagonist 1-(3-Chlorophenethyl)-3-cyclopentylpyrimidine-2,4,6-(1H,3H,5H)-trione, Compound VIII (Kang *et al.*, 2012; Huang *et al.*, 2014). As before, depolarizations under control conditions elicited rapid inward current followed by robust fast and slow outward currents (Fig. 4C, middle panel). Perfusion of 400 μM Compound VIII (50X the k_i for $Ca_V1.3$) specifically blocked both the rapid inward and rapid outward currents (Fig. 4C, bottom panel). This effect was clearer when the responses in control and Compound VIII were plotted together (Fig. 4D) for three voltage commands between −60 and −40 mV. The successful block by Compound VIII identified the rapid inward current as an L-type calcium current. The remaining slow outward current in the presence of Compound VIII was a delay followed by a single exponential rise, which could be well fit by retaining only the first and fourth terms of Eq. 5.

Based on a comparison of the control amplitude of the slow component with that in the presence of Compound VIII for four cells using Eq. 3, there is a reduction to 57.4 ± 13% (n = 4) in the slow outward current. Once again, such a result could occur if the slow outward component was itself calcium dependent, or as suggested in the BAPTA experiments, the development of the slow component was dependent on prior activation of the rapid outward current. The latter alternative could be a consequence of the accumulation of ions in the synaptic cleft following activation of the rapid outward current.

Sensitivity of the outward currents to Iberiotoxin.

The N-shape of the whole-cell I-V curve in the presence of internal 4-AP^+, and the sensitivity of the rapid outward current to TEA, calcium buffering and influx block, all indicated that the rapid outward current was a calcium-activated potassium conductance. This suggested that using Iberiotoxin (Galvez *et al.*, 1990; Candia *et al.*, 1992), IbTX, a specific antagonist of the large, calcium-activated potassium conductance, $K_{Ca}1.1$, would allow us to determine whether the partial reduction of the slow outward current was due to decreased availability of internal calcium, or a decrease in the potassium in the cleft that was associated with activation of G_{BK}. External perfusion of IbTX can be expected to suppress potassium efflux through BK channels and reduce potassium elevation in the cleft while leaving internal calcium dynamics intact. As shown for one such experiment in the voltage range −80 to 80 mV (Fig. 5A), perfusion of 200 nM IbTX dramatically decreased the total outward current, reducing it for a −10 mV command to 20.2% of its control value. In nine cells, amplitudes in the presence of IbTX ranged between 5.8% and 70.9% of control (28.3 ± 22.2%, n = 9). If the two outward currents were independent, then these results would be at odds with measurements of the relative sizes of the initial fast and final total outward currents given in the I-V curves of Fig. 1C, and, by extension, the dose-response curves of Fig. 2F. Both of those experiments were consistent with an assessment that a majority of the outward current went through the fast and slow conductances at a ratio of approximately 1:2.5. In addition, experiments involving increased calcium buffering (Fig. 4A, B) or blocked calcium influx (Fig. 4C, D, E) demonstrated that the slow component could be activated hyperpolarized to I_{BK}, or under conditions that greatly reduced the size of I_{BK}. Under the latter condition, it is possible that the fraction of G_{BK} that still activated despite reduced calcium availability was sufficient to modulate the slower outward current, and that an even greater IbTX-mediated block of G_{BK} would be necessary to reveal its downstream influence on the slower current. It is important to note that the slow component that persists in these experiments ranges between 16.9 and 57.1% (38.8 ± 15.1%, n = 7) of its control value in the presence of I_{BK}, supporting a view that I_{BK} and the subsequent elevation of potassium in the cleft dramatically alter the conductance and increase the size and speed of the slow outward current.

Effects of elevating $[K^+]_c$ on instantaneous hair cell current and tail kinetics.

A mechanism by which $[K^+]_c$ might influence the permeation of the slower conductance was suggested by the previously demonstrated effect on hair cell deactivation that accompanies elevation of $[K^+]_c$ following depolarization of either the hair cell or the afferent (Contini *et al.*, 2017). It was noted that when $[K^+]_c$ was increased, the relaxation of the tail current upon repolarization slowed. This effect could be demonstrated in experiments in which brief 10

ms pulses to 50 mV were followed by repolarization to potentials between 10 and −130 mV (Fig. 6A). In an artificial perilymph with 4 mM $[K^+]_o$, the repolarizations between 10 and −30 mV suggested that the conductance remained open, since the current during the 25 ms of the tail voltage command was not time dependent (Fig. 6A, middle panel). For repolarizations hyperpolarized to −40 mV, however, the speed of the tail current closure increased with greater hyperpolarization. Perfusion of 20 mM $[K^+]_o$, where K^+ had been substituted for Na^+ on an equimolar basis, changed the response at the onset and termination of the pulse. First, the instantaneous current in response to the initial depolarization to 50 mV was a larger fraction of the total outward current, and there was a smaller, slow incremental gain to the final value. Second, following repolarization, an initial rapid component of relaxation remained, but for a majority of the potentials the tail current flowed with little subsequent attenuation even at hyperpolarized potentials, suggesting that a major conductance had remained open.

We repeated the analysis of Fig. 1 while varying $[K^+]_o$ to quantify the effect of changes in $[K^+]_c$ on the total conductance (Fig. 6B). With an artificial perilymph of 2 mM $[K^+]_o$, the tail currents following the depolarizations relaxed to baseline prior to the initiation of the voltage command pulse 200 ms later. Four moments during the response were measured: the steady-state current just prior to the pulse, the instantaneous current at the start of the pulse, the steady-state current at the end of the pulse, and the peak of the inward tail following termination of the pulse (Fig. 6B, middle panel and inset). In contrast with the results in 2 mM $[K^+]_o$, perfusion in an artificial perilymph with 20 mM $[K^+]_o$ (Fig. 6B, bottom panel and inset) significantly changed the steady-state standing current prior to the test pulse, presumably because the tail currents following the larger pulses had yet to close prior to the next pulse. Consequently, there was a large instantaneous current at the pulse onset, although there was no significant change in the steady-state outward current at the end of the pulse. These results were visible in the corresponding I-V curves (Fig. 6C): there was negligible instantaneous current until the highest voltages in 2 mM $[K^+]_o$, but appreciable instantaneous current flowed for all potentials above −40 mV in 20 mM $[K^+]_o$. Nevertheless, the steady-state current at 0 mV was ~7.5 nA at both concentrations.

Using these data, we calculated the chord conductances at the beginning and end of each pulse (Fig. 6D) and estimated the potassium equilibrium potentials at the transitions. In 2 mM $[K^+]_o$ the instantaneous conductance at the onset reached a maximum of 5.2 nS, while that at the 25 ms steady-state peaked at 116.6 nS. The corresponding equilibria at the beginning and end of a pulse to −40 mV were −98.2 and −81.5 mV, respectively. For depolarizations to 0 mV, the equilibria were −92.1 and −60.1 mV. In contrast, when bathed in 20 mM $[K^+]_o$, the growth of the instantaneous conductance at the beginning of the pulse was apparent for potentials above −40 mV, and the fit to the data saturated at more than 40 nS at the highest depolarization. Similarly, the steady-state conductance at the end of the pulse reached a maximum of more than 150 nS at 0 mV. The estimates for the equilibria in 20 mM $[K^+]_o$ for pulses to −40 and 0 mV gave values of −82.3 and −78.2 mV at the onset of the pulse, and −63.4 and −44.6 mV in the steady-state at the end of the pulse. The results from changing $[K^+]_o$ in the bulk solution emphasize two important points about corresponding changes in potassium concentration in the synaptic cleft, $[K^+]_c$. For intracellular potassium concentrations of 125 mM, $[K^+]_i$, and extracellular concentrations of

2 and 20 mM $[K^+]_o$, we expect that the equilibria would be −106.9 and −47.4 mV for a pure potassium conductance. The equilibria at the onset of the 0 mV pulse in 2 and 20 mM given above correspond to 3.56 and 6.07 mM $[K^+]_c$, which does not reflect the full extent of the $[K^+]_o$ perfused in the bath. Of greater importance is that, at the end of the pulse, the equilibria would correspond to 12.25 and 22.27 mM $[K^+]_c$, values higher than those in either perfusate. A striking consequence of the simultaneous increase in conductance and depolarization of the equilibrium potential that would reduce the driving force, is that the product of the conductance and driving force remained constant, as reflected in the equivalent currents at 0 mV in 2 and 20 mM $[K^+]_o$.

Since these experiments were performed on cells in which both potassium currents were present, the potassium sensitivity of either remained to be demonstrated. The conductance and reversal potential for an ion channel can be manipulated by varying the intracellular and extracellular ion concentrations (Hess *et al.*, 1986). In addition, the calcium- and potassium-sensitivities of potassium channel inactivation and deactivation have been demonstrated previously (Armstrong & Hoshi, 2014; Carrillo *et al.*, 2015), although not to our knowledge for the BK channel.

Effects of elevating $[K^+]_c$ on BK and the slow outward current.

To identify the conductances with kinetics sensitive to external $[K^+]_o$ we isolated I_{BK} as above, using 15 mM 4-AP^+ in the recording pipette, and in separate experiments isolated the later, slow outward conductance by using conventional KCl-filled pipettes and externally perfusing 200 nM IbTX. Responses were recorded while bathed in 4 mM or 20 mM $[K^+]_o$ artificial perilymph (Fig. 7). I_{BK} isolation with 4-AP^+ (Fig. 7A) yielded results that could be fit with Eq. 2, using exponents of 2 and 6 as before (Fig. 3B). When potassium was elevated, there was a negligible effect on the rapid inward I_{Ca}, but a significant decrease, to 71.5% of control, in the rapid outward BK component of the current (Fig. 7A, bottom left). Based on the fits to the peak inward current, and the steady-state outward current, the I-V curves under both concentrations could be plotted along with inward I_{Ca}. The primary effect on the BK current was a rightward shift in the curve by 15.4 mV, an amount that would be appropriate for a 9.9 mM shift in the $[K^+]_c$. The tail current was extended in this cell, possibly due to a potassium-dependent relief of the 4-AP^+ block or to a BK deactivation that is sensitive to $[K^+]_o$. However, since the activation kinetics were not altered by elevating $[K^+]_o$, the latter possibility is unlikely. In all cases, the current returned to its steady-state level before the onset of the subsequent test pulse.

The slow outward current isolated by perfusing IbTX (Fig. 7B, second panel) was reduced to 50.4% of its control value. As shown previously (Fig. 5B), the rapid component of the tail current was eliminated in IbTX, leaving only the smaller and kinetically slower tail. In 4 mM $[K^+]_o$ the response was similar to that in Fig. 4B, and revealed the inward I_{Ca} followed by the slow exponential recovery of the outward current. Upon elevating potassium to 20 mM $[K^+]_o$ the currents had rapid onsets and offsets that were comparable to the slew rate of the recording electrode (Fig. 7B, third panel). The slow onset in 4 mM can be contrasted with the rapid rise and fall in 20 mM $[K^+]_o$ by overlaying the corresponding traces (Fig. 7B, bottom left). In addition, 20 mM $[K^+]_o$ elicited a large inward −725 pA shift in the holding

potential (Fig. 7B, bottom right). The steady-state I-V curves under the two conditions highlight the outward rectification in 4 mM and the comparable linearity of currents in 20 mM $[K^+]_o$, with a slight decrease in conductance for the most hyperpolarized potentials (Fig. 7B, bottom right). The shift of 35.4 mV in the zero-crossing of the two fits to the depolarizing phase of the I-V curves would be consistent with a 11.7 mM shift in the $[K^+]_c$ between the two conditions. This difference could be explained, in part, by the elimination of I_{BK} by IbTX. I_{BK} serves not only as a rapid source of K^+ into the cleft with depolarization, but also as a rapid sink for K^+ due to its inward current upon repolarization. In the absence of an I_{BK}, only the I_{slow} would serve as a slower, smaller inward current sink upon repolarization. These results may also explain the findings shown in Fig. 6; with elevated $[K^+]_o$, current through the late slow conductance is open at all potentials and is responsible for the instantaneous conductance at the onset of the voltage steps. Moreover, since the driving force is decreased by the elevation of $[K^+]_o$, the additional current flowing through an increased slow conductance may be sufficient to offset the decrease in I_{BK}.

Effects of external calcium chelation on the outward potassium currents.

In experiments analogous to those of Fig. 6, divalent substitution of Mg^{2+} or Ba^{2+} for Ca^{2+} on an equimolar basis in 4 mM $[K^+]_o$ perilymph increased the instantaneous current at the onset of a voltage step by 41 ± 28%, n = 6, and 85 ± 38%, n = 3, respectively (data not shown). These results suggested that a possible link with the potassium-sensitive potassium conductance might occur through an external divalent block or inactivation site for which Ca^{2+} had the highest affinity. To test this, we repeated the experiments in our typical extracellular solution and in a perilymph to which 5 mM EGTA had been substituted for NaCl on an equimolar basis (Fig. 8A) with the divalent concentration kept constant using 5 mM $MgCl_2$. While the rapid and slow components in the outward current were visible under control conditions, the addition of EGTA produced an inward shift of 3.37 nA in the holding current at −100 mV, and large instantaneous currents followed by growth in the slower component of the current. The instantaneous, steady-state, and tail currents were measured, and the corresponding I-V curves (Fig. 8B) were used to extract the conductances near the onset and offset of the voltage pulses. By delaying the onset measurement by ~150 μs, we could also extract the inward I_{Ca} as a voltage-dependent deviation from a linear fit to the instantaneous current (Fig. 8B, insets). Under control conditions, there was very little instantaneous current in the ± 80 mV range, and the deviation from the linear fit yielded an estimate of 300 pA for the peak inward calcium current (Fig. 8B, top, inset). When EGTA was added to the bath, the instantaneous current could again be fit by a line with a slope of 36.7 nS (Fig. 8B, bottom), and the deviation from the line suggested an amplitude that is $2/3^{rds}$ of the original I_{Ca}. The steady-state outward current showed diminished rectification, and its incremental amplitude above the instantaneous value was decreased, but the amplitude above the holding current was unchanged compared to that under control conditions. By extending the pulse to 500 ms in a different cell, the full extent of the EGTA effect was visible in the first 25 ms (Fig. 8C). Rather than a slow onset (Fig. 8C, second panel), the current reached its steady-state value limited by the slew rate of the recording (Fig. 8C, third panel). The corresponding steady-state I-V curves (Fig. 8C, bottom) showed that with prolonged depolarizations, the rectifying relationship before and after perfusion with EGTA is reduced to a nearly constant conductance with a slope of 123.8 nS.

In addition to affecting the potassium conductance under consideration, external EGTA, which theoretically should reduce the free $[Ca^{2+}]_o$ to the nM range in the bath, might affect other hair cell conductances as well. Elimination of Ca^{2+} should alter calcium entry and reduce I_{BK} activation, suggesting that what remains is the second, slow potassium conductance. Reduction of $[Ca^{2+}]_o$ would also permit movement of larger monovalent ions through the mechano-electrical transduction channels, but since the manipulation would sever tip links gating these channels, it might be expected to block their activation (Crawford *et al.*, 1991). Similarly, reduction of $[Ca^{2+}]_o$ should allow larger monovalent currents through the calcium conductance. Under such a scenario, we would expect the inward current to be roughly three to five times larger, and its U-shaped I-V curve would be shifted toward hyperpolarized potentials, with a reversal potential near 0 mV (Art *et al.*, 1993). While the shift in the reversal potential is apparent, the decrease in peak amplitude calls into question the degree to which EGTA bath perfusion was able to strip Ca^{2+} from its binding sites within the pore of the calcium channel, and the extent to which it is effective in buffering calcium transported into the cleft from hair cells surrounded by an afferent calyx. As it stands, since the I_{BK} would be at least partially decreased by external Ca^{2+} chelation, it is likely that it is the slowly activating potassium-sensitive potassium conductance (Fig. 7B) whose I-V is linearized by lowering the effective $[Ca^{2+}]_c$.

The fact that either elevation of $[K^+]_o$ or reduction of $[Ca^{2+}]_o$ decreases the I-V rectification of the potassium conductance raises the possibility that the shape observed under control conditions might be determined by the ion sensitivity of the more external selectivity filter, rather than by the inherent voltage sensitivity of an internal channel gate. In such a circumstance, monovalent and divalent concentrations within the cleft would dynamically control permeation by interactions with this filter. The constellation of conductances active at a given potential would reflect both the inherent voltage-sensitivity of the conductances, and the voltage-dependent changes in ion concentrations in the cleft. In principle, this would result in conductance *vs* voltage activation curves that would explicitly depend on the holding potential, and by extension on the steady-state ion concentrations in the synaptic cleft.

Potential-dependent differences in hair cell current activation – the effect of $[K^+]_c$.

With hair cell and afferent held at −100 mV, the voltage-dependent potassium conductances are deactivated in both cells. The inward current through the mixed-conductance HCN channels in the afferent (Meredith *et al.*, 2012), and to a lesser extent the hair cell (Horwitz *et al.*, 2011), would be responsible for drawing the extracellular bath into the synaptic cleft. Assuming an equal density of HCN channels on the inner and outer faces of the calyx afferent, then half of the 913 pA standing inward current at −100 mV (Fig. 9A, bottom panel, dashed line, triangle) would be drawn into the synaptic cleft and would flow into the calyx inner-face HCN channels. Based on ± 10 mV commands from the holding potential, the inward 115 pA in the hair cell (Fig. 9, middle panel, horizontal line) resulted from a 1.13 nS leak to 0 mV, which would be consistent with the sum of open transduction and electrode seal conductances at this potential.

Under these conditions, depolarization of the hair cell to −70 mV gave rise to the first measurable outward current, and upon repolarization, the zero-crossing of the chord conductance was consistent with a $[K^+]_c$ of 4 mM, equivalent to the concentration in the bath. For larger hair cell depolarizations up to −40 mV (Fig. 9A, middle panel), there is little instantaneous current, and over the duration of the 500 ms pulse the current grew to a peak, partially adapted, and then increased with slower kinetics to a final value of 931 pA above the steady state. The zero-crossing of the chord conductance upon repolarization, −52 mV, was consistent with increasing $[K^+]_c$ to 16.7 mM over the course of the pulse to −40 mV. The inherent potassium sensitivity of the afferent HCN channels was responsible for the associated systematic increase in the mixed Na^+ and K^+ inward current (Fig. 9A, bottom panel) that accompanied depolarization of the hair cell (Contini *et al.*, 2017). At the end of the depolarization of the hair cell to −40 mV, the final amplitude of the afferent inward current was 145 pA greater than that at the holding potential.

With hair cell hyperpolarization to −120 mV, a slowly-activating inward current was observed, which increased by 73 pA by the end of the 500 ms pulse. This reflected the previously reported hair cell I_h (Horwitz *et al.*, 2011), and the suppression of −103 pA at −150 mV by 200 μM ZD7288, an HCN channel blocker (Fig. 7F in (Contini *et al.*, 2017)). Measuring the conductance as before (Fig. 1C), the G-V plot for a holding potential of −100 mV (Fig. 9A, inset) was fit by a sigmoid with minimum, g_o = 0.4 ± 2.9 nS (coeff. ± S.D.) and maximum, g_{max} = 145.3 ± 4.8 nS. The total conductance was half activated at −59.4 ± 0.8 mV and had a rate of 5.7 ± 0.7 nS•mV^{-1} at the half-activation voltage.

In general, isolated hair cells in artificial perilymph are probably hyperpolarized from their true values because the depolarizing transduction currents can be mechanically compromised during isolation, and/or because the artificial perilymph has a higher $[Ca^{2+}]_o$ than the 300 μM in native endolymph at the transduction pole *in vivo* (Salt *et al.*, 1989). High levels of calcium would significantly reduce the transducer conductance and the standing inward current (Crawford *et al.*, 1991). In addition, the mean resting potentials *in vivo* under conditions of asymmetric salt solutions bathing apical and basolateral surfaces are not known since the thick cartilaginous stroma subjacent to the epithelia precludes recordings from hair cell and afferent *in situ*. Lacking these data, we compared the responses of synaptic pairs at −100 mV to those at potentials near, or depolarized to the values reported for isolated mammalian hair cells in gerbil, −71 mV (Rennie & Correia, 1994), and mouse, −79.5 mV (Rusch & Eatock, 1996), but still hyperpolarized to the −50.1, and −62 mV values reported in hair cell and afferent microelectrode recordings of the intact turtle auditory papilla (Crawford & Fettiplace, 1980).

When hair cell and afferent were held at −70 mV (Fig. 9B), the responses were markedly different from those observed at −100 mV, but resembled many of the features previously reported for solitary turtle vestibular hair cells held at similar potentials (Brichta *et al.*, 2002). The large instantaneous currents at the onset of the voltage command were linearly related to the voltages, with a conductance of 26.7 nS open at the holding potential. The sole deviation from linearity occurred with the −120 mV command, where the bandwidth of the recording system underestimated the peak current, given its rapid deactivation. For voltage commands more hyperpolarized than −90 mV, the current deactivation relaxed to a limiting

inward current of −121 pA (Fig. 9B, middle panel, horizontal line), similar to the prior steady-state leak to 0 mV at −100 mV. Thus, at the holding potential, the 128 pA outward current was 249 pA above the limiting value. This would require a driving force of 9.3 mV through the 26.7 nS conductance, or an E_K = −79.3 mV, which would correspond to elevating $[K^+]_c$ to 5.8 mM in the steady state. The presence of instantaneous currents with elevation of $[K^+]_c$ mirrors the results with elevated $[K^+]_o$ shown in Figures 6 and 7. At −70 mV, the time constants for $I_{K(LV)}$ deactivation following depolarizations to −50 and −40 mV were 39 and 40.6 ms respectively, both considerably slower than the mean time constant for return to the steady-state current, 25.8 ± 2.7 ms, following hyperpolarizations between −90 and −120 mV. These results were consistent with voltage-dependent changes in $[K^+]_c$, which in turn regulated a hair cell conductance. The G-V plot for a holding potential of −70 mV (Fig. 9B, inset) was fit with a sigmoid where g_o = 2.3 ± 1.1 nS and g_{max} = 39.8 ± 1.5 nS. This indicates that, when held at −70 mV, more than 105 nS of the total conductance was inactivated in comparison with holding at −100 mV. In addition, at −70 mV, the conductance was half activated at −75.2 ± 1.4 mV, a potential more hyperpolarized by 15.8 mV from the value measured when holding the cell at −100 mV. Finally, the voltage sensitivity was 1.64-fold less, with a rate of 9.4 ± 1.1 nS•mV^{-1} at the half-activation potential.

When held at −70 mV, the evoked afferent response also departed from the responses obtained at −100 mV (Figs. 1A, bottom panel; 9A, bottom panel). The standing inward current at −70 mV was reduced to 303 pA, or 33.2% of its value at −100 mV (Fig. 9B, bottom panel, dashed line, inverted triangle), and the 118 pA modulation of the inward current about the holding current was bidirectional. When the hair cell was hyperpolarized from −70 mV, the standing potassium efflux into the cleft was reversed, and the resultant lowering of $[K^+]_c$ reduced the evoked inward current through HCN channels. Turning off a standing inward current appeared as a relative outward current with respect to baseline in the afferent (Fig. 9B bottom panel, expanded in 9D, third panel). When the hair cell was depolarized, potassium efflux increased as before, which elevated $[K^+]_c$ and increased the inward current from its steady-state value.

Equivalent experiments clamping the hair cell at −100 mV and the afferent at −70 mV yielded hair cell G-V curves similar to those obtained when holding both at −100 mV. Under these conditions, the G-V curve had g_o = 1.6 ± 1.6 nS, which was indistinguishable from the leak to zero, and the g_{max} was reduced by 23% to 112.0 ± 3.0 nS. The half-activation voltage of −61.8 ± 0.8 mV and rate of 6.1 ± 0.7 nS•mV^{-1} were only slightly more hyperpolarized and slower than the results obtained when both hair cell and afferent were held at −100 mV.

In the population as a whole, when hair cells and afferents were both held at −100 mV, the mean maximum conductance was 151.7 ± 103.7 nS (n = 22) and the half activation of the total outward current was −59.3 ± 9.9 mV. This contrasted sharply with the maximum total conductance of 37.1 ± 19.2 nS (n = 19) and a half-activation voltage of −81 ± 14.3 mV obtained when both hair cell and afferent were held at −70 mV, suggesting that on average 74% of the conductance was inactivated at the more depolarized potential. Moreover, when hair cell and afferent were held at −70 mV, the hyperpolarized range of half-activation voltage of the total current suggested that the slowly activating, potassium-sensitive current in our study is likely equivalent to the low-voltage-activated potassium conductance, $G_{K(LV)}$

previously reported in solitary cells (Rennie & Correia, 1994; Rusch & Eatock, 1996; Meredith & Rennie, 2016). Taken together, these data indicate that the activation, inactivation, and deactivation characteristics of the outward hair cell current were largely set by the holding potential, which determined the $[K^+]_c$ resulting from potassium efflux through $G_{K(LV)}$ at more hyperpolarized potentials, and a combination of $G_{K(LV)}$ and G_{BK} at potentials depolarized to −50 mV, based on I_{Ca} and I_{BK} activation curves.

Modeling of potassium-sensitive relief from block, and the kinetics of inactivation/deactivation.

In prior studies, $I_{K(LV)}$ has been characterized as having single (Chen & Eatock, 2000) or multiple (Spaiardi *et al.*, 2017) voltage-dependent 'closed-to-open' transitions. In our experiments, the pharmacologically isolated $I_{K(LV)}$ had exponential growth and decay, and sigmoidal G-V curves (Fig. 9B, inset) that were sensitive to $[K^+]_c$ and $[Ca^{2+}]_c$. We considered as an alternative that the apparent voltage-dependence of its activation and deactivation could be modeled as a simple two-state binding reaction, with single open and closed states,

$$\beta + O \underset{k}{\overset{\mu}{\rightleftarrows}} \beta O, \tag{6}$$

where O denoted a conducting channel, βO was nonconducting, and κ and μ were voltage-dependent rate constants that resulted from voltage-dependent changes in $[K^+]_c$ and $[Ca^{2+}]_c$. The derivation for outward rectification was analogous to that previously used to model an auditory hair cell inward rectifier (Goodman & Art, 1996a), where we assumed that an apparent dissociation constant was given by the ratio of the backward and forward rate constants, having a voltage dependence of the form

$$\kappa/\mu = K_B \bullet \exp\left[\left(V - V_B\right)/V_e\right], \tag{7}$$

where K_B was the apparent dissociation constant at V_B, and V_e was the voltage dependence. In the steady-state, the probability, p, that the channel was unblocked at a voltage could be found by setting

$$dp/dt = (1 - p)\kappa - p\mu[\beta]_o = 0, \tag{8}$$

which yielded

$$p_\infty = \kappa/(\kappa + \mu[\beta]_o). \tag{9}$$

Substitution of the voltage dependence of the apparent dissociation constant into the equation for steady-state open probability yielded

$$p_{\infty} = \frac{1}{1 + \left({}^{[\beta]_o}\!/_{K_B}\right) \bullet \exp\left\{\frac{-V + V_B}{V_e}\right\}}. \quad (10)$$

Assuming that the underlying conductance in the absence of block was constant over the voltage range of interest, then the current through the outward rectifier would be given by

$$I_{\infty} = g_{max} \bullet N_{shift(\infty)} \bullet \left(V - E_{k(-100\,mV)}\right) \bullet \frac{1}{1 + B \bullet \exp\left\{\frac{-V + V_B}{V_e}\right\}}, \quad (11)$$

where g_{max} was the limiting conductance, $N_{shift(\infty)}$ was the fractional shift in the equilibrium potential in the steady state for each mV of depolarization, $E_{k(-100\,mv)}$ was the potassium equilibrium potential in the cleft at the holding potential (−100 mV), B was a dimensionless constant equal to $[\beta]_o/K_B$, V_B was the midpoint for the block, and V_e was the voltage dependence of the block. Eq. 11 was then used to fit the steady-state I-V curves in 2 and 20 mM $[K^+]_o$ (Fig. 9C) for the cell of Fig. 7B that had I_{BK} selectively blocked with IbTX.

Elevation of $[K^+]_o$ from 4 to 20 mM had the expected result of a modest increase in the maximum conductance, g_{max}, from 12.5 to 14.6 nS, and a rightward shift in the reversal potential, E_k, from −77.3 to −33.5 mV. The latter would correspond to values of 6.3 mM and 34.2 mM for $[K^+]_c$, which in each case exceeded the values in the bath, $[K^+]_o$, by more than 50%. This suggested that in the steady-state, the intra-cleft potassium concentration, $[K^+]_c$, often exceeded that in the bulk solution. It is also apparent (Fig. 9C) that rectification was drastically reduced in elevated $[K^+]_o$, with voltage-dependence, V_e = 14.2 mV in 4 mM $[K^+]_o$ depreciating nearly four-fold, to 48 mV, in 20 mM $[K^+]_o$. The effect of elevating $[K^+]_o$ was also consistent with the notion that K^+ accumulation competes with blocking or inhibition, and the half-blocking voltage, V_B, was hyperpolarized from −50.3 mV in 4 mM to −73.3 mV in 20 mM $[K^+]_o$. In such a scheme, the dimensionless ratio B, which represents the concentration of the blocking particle over the half-blocking dose, was reduced by 60%, from 0.433 to 0.175, suggesting that elevation of $[K^+]_c$ effectively decreased the block.

Overall, these fits support a model in which elevated $[K^+]_c$ relieves a permeation block, either by an allosteric interaction through its own binding site, or by interfering with an external-face divalent binding site that affects permeation through the selectivity filter of the pore. The proposed model is also consistent with studies of other potassium conductances, which found that rates of potassium current inactivation and deactivation increased in the presence of elevated $[Ca^{2+}]_o$, and were slowed by elevation of $[K^+]_o$ (Armstrong & Hoshi, 2014; Carrillo *et al.*, 2015). Studying hair cell current deactivation was complicated by the apparent potassium-sensitivity of the conductance in question. The slow deactivation of the total hair cell potassium current at −100 mV was comparable in duration to the post-synaptic inward current in the afferent fiber (Fig. 1A, bottom). This suggested that $[K^+]_c$ elevation followed the time course of the afferent tail, since the increase in the mixed Na^+ and K^+ afferent current is largely due to the potassium-sensitivity of the underlying HCN channels

(Contini *et al.*, 2017). As an alternative, we examined the kinetics of current deactivation when hair cells were hyperpolarized from a holding potential of −70 mV, a value hyperpolarized to the voltage required to activate I_{Ca} and I_{BK} and likely to minimize the I_{BK} contribution to the deactivation time course. Consistent with the results in Fig. 1, deactivation of the inward tail currents (Fig. 9D, second panel) followed a time course that conveyed an apparent outward current in the afferent reflecting a decrease in its standing inward current (Fig. 9D, third panel). Moreover, the large amplitude of the inward hair cell current at these potentials suggests that much of the time-dependent removal of K^+ from the cleft over the short-term flows back into the presynaptic hair cell through this conductance. The voltage-dependent time constants of deactivation were well fit by single exponentials (Fig. 9D, second panel, dashed lines), and the time constants for four cells were pooled to determine a mean at each voltage (Fig. 9D, fourth panel).

For our proposed model, in which elevated $[K^+]_c$ relieves a block, the voltage-dependence of time constant, τ, should be equal to the reciprocal of the sum of the forward and backward rate constants whose voltage dependence is given in Eq. 7. Explicitly for deactivation upon repolarization,

$$\tau = \frac{1}{\mu \bullet \left(1 + K_B \bullet \exp\left\{\frac{-V + V_B}{V_e}\right\}\right)}, \tag{12}$$

where the variables are defined in Eq. 7. These data yielded mean time constants of deactivation (Fig. 9D, fourth panel) that systematically decreased from 36.7 ms at −91.7 mV to 14.9 ms at −122.9 mV, and could be optimally fit (solid black line) using parameters μ = 0.027 $M^{-1}s^{-1}$, K_B = 2.135 M, V_B = −125 mV, V_e = 6.2 mV.

Comparison of hair cell and afferent responses at two voltages, and the implication for multiplexed modes of synaptic transmission.

In a majority of our experiments, the hair cell and afferent were held at −100 mV, a potential that forced conductances of interest toward closed states farthest from a closed-to-open transition and separated the conductances kinetically. When depolarized to −60 mV or above, the slower-activating $I_{K(LV)}$ could be observed as the first current to be activated (Fig. 1B). With depolarization to −50 mV, a small I_{Ca} could be observed, and the activation of $I_{K(LV)}$ was both faster and larger. For depolarizations to −40 mV and above (Fig. 1A, inset; Fig. 10A, middle panel), all three currents were visible, and $I_{K(LV)}$ was the dominant component of total outward current. The experiments that blocked I_{BK} (Figs. 4 & 5) and thereby reduced $I_{K(LV)}$ demonstrated that I_{BK}-mediated potassium efflux into the cleft elevated $[K^+]_c$ to concentrations that rapidly unblocked additional $G_{K(LV)}$. Thus, at potentials wherein I_{Ca} was activated and promoted vesicle fusion, I_{BK} would also be activated, and therefore a combination of G_{BK} and $G_{K(LV)}$ would be responsible for elevating $[K^+]_c$.

In contrast, when the cells were held at −70 mV, the large instantaneous hair cell currents through the dominant $G_{K(LV)}$ mask the underlying inward I_{Ca} and outward I_{BK} that were also activated with depolarization (Fig. 10B, middle panel). With the exception of the rise in

the additional outward current after the initial jump, or in the deactivation upon repolarization, the contributions of these currents were less apparent than they were when cells were held at −100 mV. Hyperpolarizations following depolarization to −30 mV or more typically gave two-component tail currents with time constants of 2.5 and 16.3 ms, where presumably, as in Fig. 2, the faster corresponded to the deactivation of I_{BK}, and the slower corresponded to the deactivation of $IK_{(LV)}$.

In life, both hair cell and afferent in equilibrium are depolarized from −100 mV, though for reasons enumerated above, their precise resting potentials are unknown. At −70 mV, the dynamics of the coupled hair cell and afferent response were very different from those illustrated in Fig. 1A, and suggested that in addition to the quantal transmission and ion accumulation in the cleft that couple the cells, there is a direct resistive path between the two that exists when $[K^+]_c$ is elevated. Examples of slow afferent responses resulting from ion accumulation when hair cell and afferent were held at −70 mV have been published previously. They demonstrated the reciprocal interaction between the two mediated by the dynamic changes in $[K^+]_c$ due to ion flux from either hair cell or afferent (Contini *et al.*, 2017). That study characterized the hair cell – afferent interaction over hundreds of ms, as opposed to focusing on the first few ms of the response. Moreover, in the present study we have demonstrated that at −70 mV, there was an average basolateral conductance of 24.7 nS through which the transduction currents would flow out of the hair cell as I_K, into the synaptic cleft, and rapidly elevate $[K^+]_c$. A typical semicircular canal hair cell in the central region has a capacitance of 10 pF, of which ~40% represents the stereociliary bundle and 60% the basolateral surface. Assuming 100 μm^2/pF, the basolateral surface corresponds to ~600 μm^2. The width of the cleft in unfixed material is estimated to be ~65 nm (Lim *et al.*, 2011), giving a volume for the cleft on the order of 39 fl. Currents of 1 nA (~6 x 10^9 monovalent ions/s) flowing into this volume through the $G_{K(LV)}$ and G_{BK} on at the resting potential would be expected to generate mM changes in $[K^+]_c$ within ~10 ms, omitting flux out of the cleft through the afferent or the apical gap between afferent and hair cell. This, in turn, would change the driving force on any afferent potassium channels that are open at rest, and change the total current flowing into the afferent. An elevation of $[K^+]_c$ would increase inward current through HCN channels and decrease outward current through open potassium channels in the afferent, and the combinaton of the two would be manifest as an increase in total inward current (Contini *et al.*, 2017).

When both cells are held at −100 mV, the triphasic response in the hair cell (Fig. 1A, inset, and 10A, middle panel) produced a stereotypical sigmoidal increase in the inward current in the afferent (Fig. 1A, bottom panel; Fig. 10A, bottom panel). This differed from the result when both hair cell and afferent were held at −70 mV (Fig. 10B). In the hair cell, the initial response was an instantaneous jump from the holding current, followed by a small decrement, and then ultimately an increase in additional outward current (Fig. 10B, middle panel). The response in the afferent was a corresponding ‘instantaneous jump,’ τ = 32 μs (475 ± 479 μs), followed by an exponential increase of the inward current (Fig. 10B, bottom panel; expanded in Fig. 10C). Based on the volume of the synaptic cleft calculated above, time constants of ~30 – 1000 μs are too fast to be explained by the tens of milliseconds time course associated with changes in $[K^+]_c$ and changes in the driving force through open afferent potassium channels. That said, in this case the inward afferent current jump

represents only about 1 – 2% (1.91 ± 2.8%, n = 17) of the outward basolateral current from the hair cell, suggesting that, by Kirchhoff's current law, a majority of the current flows either directly into the extracellular space in regions not surrounded by the afferent or via the opening of the synaptic cleft near the apex of the hair cell. The percentage into the afferent would be dependent on the ratio of the resistances of the cleft and afferent membrane (Fig. 12B). While small, this percentage is not insignificant; the resistive coupling of 350 pS in Fig. 10B (522 ± 577 pS, n = 17) is comparable to that between adjacent mammalian cone photoreceptors (DeVries *et al.*, 2002). By implication, given a finite resistance out of the synaptic cleft into the bath, the large potassium-sensitive conductances open around the resting potential in hair cell and afferent create a dynamic potassium-sensitive resistive coupling between pre- and postsynaptic cells. Added to the quantal transmission and ion accumulation previously characterized, such a resistive coupling constitutes a potential third form of transmission multiplexed at the synapse.

Discussion:

Synaptic apposition and ionic modulation of modes of transmission.

Potassium efflux into the synaptic cleft from either hair cell or calyx afferent elevates $[K^+]_C$, results in depolarization of the synaptic pair, and enhances the speed and fidelity of quantal transmission (Contini *et al.*, 2017). This effect was clear because of the apposition between pre- and postsynaptic cells, and the resulting large synaptic volume. We expect that in principle these effects will obtain at smaller synapses throughout the nervous system, though the small volumes and high-speed changes in ion concentration would make reliable measurements by our technique more challenging.

In the context of hair cell to afferent transmission, three outstanding questions remained concerning mechanisms that regulate hair cell potassium efflux over a physiologically relevant range and the implications of potassium-sensitive conductances for multiplexed modes of synaptic transmission. First, to keep the hair cell near the threshold for calcium influx and vesicle fusion, the potassium currents and efflux from the hair cell would need to be adjusted so that the $[K^+]_C$, the effective E_K, and the resulting outward current, I_K, matched the sum of the inward calcium, I_{Ca}, and transducer, I_{MET}, currents near the threshold for quantal transmission (Fig. 12A). Second, the regulation of basolateral conductances must be such as to compensate for the dynamic elevations in $[K^+]_C$ and associated reduction in driving force to prevent adaptation in the outward currents. Third, with large potassium-sensitive conductances open near the resting potential, any elevation of $[K^+]_C$ will increase the resistive coupling between hair cell and afferent, thereby affording an additional direct mode of transmission that depends on the level of recent cellular depolarization.

To address the first two questions, our experiments were designed to kinetically and pharmacologically separate the underlying hair cell conductances responsible for elevating $[K^+]_C$. Specifically, we were interested in their inherent voltage dependence, as well as their sensitivities to internal and external cation concentrations. Prior experiments suggested that the kinetics and open probability of at least part of the hair cell potassium conductance were sensitive to external potassium, and channels would remain open upon elevation of $[K^+]_C$

(Contini *et al.*, 2017). To assess any interdependence between these conductances, our experiments used dual-recording of hair cell and afferent with an approach to each cell that preserved the integrity of the synaptic cleft. Preservation of this intercellular space was paramount, since it is the context for the dynamic changes in ion concentration in which the basolateral hair cell conductances function (Vincent *et al.*, 2018).

Cell isolation would also miss conductance interdependencies that result from their functioning in a restricted, dynamic environment *in vivo*. Studies on solitary type I hair cells generally assume that the ionic environment is constant and reflects the ion concentrations of the bulk solution (Rennie & Correia, 1994; Rusch & Eatock, 1996; Brichta *et al.*, 2002). Recent experiments on nominally isolated, solitary type I cells may call into question such an assumption. Measurements of ion accumulation based on the shift in apparent E_K suggest that typically at least some of the afferent calyx adheres to type I hair cells, and solitary cells without potential sites of ion accumulation constituted less than 16% of the population of isolated cells (Spaiardi *et al.*, 2017).

Kinetic separation of three currents

In the majority of these experiments, hyperpolarization of hair cells to a holding potential of −100 mV was used to turn off conductances that open upon depolarization, and to force them into a deep closed state furthest from any closed-to-open transition. Subsequent depolarizations from this potential displayed three kinetically distinct currents that could be identified within the first five milliseconds (Fig. 1A, inset): a rapid inward current with a U-shaped I-V curve, a rapidly-activating outward rectifier, and a second, more slowly-activating outward rectifier. The activation voltages for these currents were remarkably similar, with activation occurring for potentials depolarized from −70 mV, which suggests that all three conductances are active at the potential viewed as the nominal resting potential for type I hair cells. The activation kinetics of the three currents had apparent voltage dependence, and for the largest depolarizations, the two outwardly rectifying currents activated contemporaneously.

The kinetics and voltage range of activation of the inward current were similar to that previously characterized for the inward calcium current in rat vestibular (Bao *et al.*, 2003) and turtle auditory (Art *et al.*, 1993) hair cells, a point that was supported by its block by the $Ca_V1.2/Ca_V1.3$ blocker, Compound VIII (Kang *et al.*, 2012). That said, the average amplitude (320 ± 53 pA, n = 12) was nearly 500% larger than the I_{Ca} previously reported for the smaller type I vestibular hair cells in the rat (Bao *et al.*, 2003). The voltage-dependent kinetics and the voltage range of activation of the rapidly-activating outward rectifier were similar to the values for a delayed rectifier previously described in birds and rodents (Rennie & Correia, 1994; Rusch & Eatock, 1996), though its block by IbTX in our experiments demonstrates that it is a large calcium-activated potassium channel, $K_{Ca}1.1$, that gives rise to I_{BK}.

The major difference between our experiments when holding both hair cell and afferent at −100 mV and prior results on solitary cells was the absence of a current whose activation was initiated near −90 mV, and had a half-activation in the −80 to −70 mV range (Rusch & Eatock, 1996; Brichta *et al.*, 2002). By contrast, when activated from holding at −100 mV,

the second, slowly-activating rectifier began to strongly activate at potentials depolarized from −68 mV and was half-activated at −59 mV. Additionally, we failed to observe the wide range of activation voltages previously reported for this current (Rusch & Eatock, 1996; Brichta *et al.*, 2002), which had led to the suggestion that the major type I hair cell conductance might be under the control of second messengers (Chen & Eatock, 2000). We believe that these discrepancies may be explained in part by considering the potassium and calcium sensitivity of this conductance and the mechanisms for controlling its permeation. Since it may constitute 75% or more of the total outward current, for consistency with this being the dominant outward current in the literature, we designated it $I_{K(LV)}$ in spite of activation at potentials significantly depolarized from the E_K in the bath.

The two outward rectifiers, I_{BK} and $I_{K(LV)}$, comprised varying proportions of the outward current over a 25 ms voltage command to different potentials. For smaller depolarizations, I_{BK} was dominant, and $I_{K(LV)}$ began to develop toward the end of the pulse. For larger depolarizations, the activation of I_{BK} was progressively subsumed by the more rapid activation of $I_{K(LV)}$. Comparison of the early and final I-V curves for the outward current (Fig. 1C) suggested that I_{BK} contributes approximately 25% of the total current into the cleft at a potential of 0 mV. As with prior experiments, the chord conductance between the final outward current and the inward tail upon repolarization could be used to calculate the voltage-dependence of the sum of these currents, and using the zero-current crossing, the reversal potential and an estimate of E_K could be calculated as well. As with extended 500 ms voltage commands, the 25 ms depolarizations of the hair cell gave minimally adapting outward currents that significantly raised the $[K^+]_c$.

The contemporaneous response in the calyx on the 25 ms time scale (Fig. 1A, B) revealed that the fine structure for the development of inward current in the afferent mirrored the activation of the two hair cell currents. Since activation of an inward current in the calyx is dependent on elevating $[K^+]_c$, the two phases observed in the growth of the afferent inward current demonstrate that both I_{BK} and $I_{K(LV)}$ contribute to the elevation of $[K^+]_c$. In general, the relative amplitudes of the two phases in the calyx reflected differences in the proportion of I_{BK} and $I_{K(LV)}$ in different hair cells. As noted in Results, this analysis also allowed us to demonstrate the effect of the currents associated with hair cell depolarization on $[K^+]_c$, and that the rate of elevation of potassium in the cleft was voltage-dependent (Fig. 1E).

Pharmacological separation of the currents and their dependencies

To assess the effect of different reagents on kinetically distinct currents, pharmacological dissection of hair cell currents was performed from a holding potential of −100 mV. The alternative of studying them from a holding potential of −70 mV was rejected since this is a potential near which all three currents start to activate, and near which they begin to overlap kinetically. Under that condition, dissection of overlapping currents would need to rely on subtracting currents at the same potential in the presence of different blockers. One concern was that true difference currents could not be reliably calculated, since the residual access resistance and wide variation in total current under different blocking conditions would result in significantly different potentials reached by the cell for identical voltage commands. A second concern was that relying on such difference currents would make it more difficult

to characterize the half-blocking dosages of the wide-spectrum potassium channel blockers 4-AP^+ and TEA-Cl for each conductance, and consequently hamper our ability to estimate the fractional reduction of each current resulting from a particular concentration of either drug. The third and most important concern was that, by not studying the activation from −100 mV and exploiting the separable kinetics of the three currents, we would fail to identify the dependency on intra- and extracellular ionic concentration that affect permeation in these conductances. It was for this reason that we also began the separation of the currents with the one that was slowest to activate, and might be dependent on the prior currents.

Previously, the separation of voltage-dependent from calcium-dependent potassium currents in auditory hair cells in the turtle relied on differential sensitivities to 4-AP and TEA that were inversely related and whose half-blocking doses for each reagent differed by more than an order of magnitude (Goodman & Art, 1996b). In the present experiments, we exploited the fact that at pH 7.2 in the internal solution, 4-AP converts to 4-AP^+, and the pyridinium form is retained within the cell where, based on the reduction of the early *vs* late outward currents, it half-blocks $K_{(LV)}$ and BK channels at 233 μM and 8.85 mM respectively. This disparity in blocking doses suggested that a concentration of 15 mM 4-AP^+ would reduce the $I_{K(LV)}$ to 2% of its value, and allow us to analyze the response of the residual 37% of the I_{BK} in isolation.

With 15 mM 4-AP^+ in the hair cell recording pipette, the current profile upon depolarization from −100 mV was reduced to a single rapid inward current followed by a rapid outward current. The reduction in current amplitude under these conditions reduced the voltage drops across the access resistance, and larger depolarizations to 80 – 100 mV could be achieved. These depolarizations revealed N-shaped I-V curves, with a reduction in outward current above 50 mV, that were reminiscent of calcium-activated potassium currents (Meech & Standen, 1975). Results from cell-attached, single-channel recordings of large, 170 pS, channels whose probability of opening decreased when $[Ca^{2+}]_i$ was reduced (Lapeyre *et al.*, 1993), were consistent with calcium-activated potassium channels covering the basolateral type I hair cell membrane. The N-shape of some I-V curves was noted previously (Eatock & Hutzler, 1992; Rennie & Correia, 1994), and was later identified in a sub-population of type I hair cells in the striola and medial extrastriola of the turtle utricle, leading to the suggestion that, in addition to the dominant $I_{K(LV)}$, currents with more depolarized half-activations in this group might be calcium-activated (Moravec *et al.*, 2006). As expected, the perfusion of TEA (Fig. 3) reduced the amplitude of the I_{BK} in a dose-dependent manner for a single binding site, with a half-blocking dose of 460 μM, very near that of turtle auditory hair cells (Fig. 3D). Concentrations of 6 mM TEA reduced I_{BK} to 7.1% of its value, revealing that I_{Ca} was in fact maintained for the duration of the voltage command and was not a transient inward current (Fig. 1).

By increasing calcium buffering in the hair cell using KCl electrodes in which 30 mM BAPTA was substituted for K^+ on an equimolar basis (Fig. 4), I_{BK} was blocked and the average delay and time constant of the $I_{K(LV)}$ were increased. This raised the possibility that $I_{K(LV)}$ was dependent on one or both of the two prior currents, I_{Ca} and I_{BK}. To examine the requirement for calcium entry on these two currents in a single cell, Compound VIII was used to block $Ca_V1.3$, the major hair cell I_{Ca} (Zidanic & Fuchs, 1995; Green *et al.*, 1996;

Schnee & Ricci, 2003). Compared to control, I_{Ca} and I_{BK} were blocked as expected, and the residual $I_{K(LV)}$ was slowed and reduced in amplitude as well (Fig. 5). Such results suggested that either $I_{K(LV)}$ had a higher calcium affinity than I_{BK}, allowing it to activate under conditions of severely reduced $[Ca^{2+}]_i$, or that it required the activation of I_{BK} to respond maximally.

To distinguish between these alternatives, IbTX was used to selectively block I_{BK}, while leaving I_{Ca} intact. Based on our prior kinetic analysis and the relative amplitudes of the early and late outward currents, we expected the majority of the outward current to be carried by $I_{K(LV)}$, as suggested in other studies (Rusch & Eatock, 1996; Brichta *et al.*, 2002). If I_{BK} and $I_{K(LV)}$ were independent, then we would expect that application of IbTX would leave I_{Ca} and $I_{K(LV)}$ intact, which in the average case would mean that ~70% of the outward current would remain. The surprising result following application of IbTX and the elimination of I_{BK} was that the remaining outward current could be as little as 5.8% of the original outward current, rather than the expected 60 – 80% (Fig. 6B). Since, as with the Compound VIII experiments on the I_{Ca}, these measurements with and without toxin were on the same cell, and not population studies, this led to the necessary conclusion that $I_{K(LV)}$ was dependent for its complete activation not on I_{Ca} and $[Ca^{2+}]_i$, but rather on I_{BK} and a flux of K^+ into the cleft. In retrospect, this unexpected result was consistent with our kinetic experiments (Fig. 1), in which the late $I_{K(LV)}$ activated more rapidly and became larger as the early I_{BK} increased with depolarization. It was also consistent with our prior study (Contini *et al.*, 2017) demonstrating that a component of the hair cell potassium conductance deactivated more slowly in elevated $[K^+]_c$.

Potassium and calcium sensitivities of $I_{K(LV)}$

Elevation of $[K^+]_c$ would be expected to shift the reversal potential (Curtis & Cole, 1942), increase the single channel conductance (Hladky & Haydon, 1972), and according to the GHK equation (Goldman, 1943; Hodgkin & Katz, 1949) decrease rectification of the I-V curves as $[K^+]_c$ approaches $[K^+]_i$. So, the possibility remained that the slowing of the deactivation and the linearization of the $I_{K(LV)}$ I-V curve might be expressions of these phenomena as a result of elevated $[K^+]_c$ and its slow removal from the cleft. Indeed, in experiments in which both I_{BK} and $I_{K(LV)}$ were present, elevation of $[K^+]_o$ led to an increase in the total conductance on at the holding potential, and a slowing of the deactivation of the tail currents upon repolarization (Fig. 6B). Examination of each conductance in isolation demonstrated that the decrease in amplitude of I_{BK} was consistent with a primary effect due to a shift in the reversal potential, with modest effects on the degree of rectification of the I-V curve or the kinetics of deactivation (Fig. 7A). A retention of most of the rectification in I_{BK} was not unexpected, given that its activation is dependent on both I_{Ca}, with its effect on $[Ca^{2+}]_i$, and on voltage. On the other hand, raising $[K^+]_o$ to 20 mM, which based on chord conductances would raise $[K^+]_c$ to 17 mM, resulted in a $G_{K(LV)}$ that was open at all but the most hyperpolarized potentials (Fig. 7B, lower right). This dramatic decrease in rectification of the $G_{K(LV)}$ I-V was far greater than would be expected by the GHK equation for a ratio of $[K^+]_i/[K^+]_o$ of 4:1. The loss of deactivation upon hyperpolarization also suggested that control of permeation was not primarily a voltage-dependent phenomenon. This was in stark contrast to models of $I_{K(LV)}$ based on recordings from nominally solitary cells described as

having single (Chen & Eatock, 2000) or multiple (Spaiardi *et al.*, 2017) voltage-dependent 'closed-to-open' transitions. In those experiments, an apparent voltage dependence would critically depend on an external K^+ shell where any accumulation would be driven by voltage-dependent currents such as I_{BK}. This might occur because portions of the afferent membrane were retained in the hair cell isolation (Spaiardi *et al.*, 2017), or be due to minimally-stirred boundary layers at the cell membrane at the bottom of the recording chamber (Hodgkin & Horowicz, 1959; Kim *et al.*, 2019). In the first case, depending on the degree of membrane apposition, the voltage range of half-activation could vary by tens of millivolts. In the second case, the rate of activation of $I_{K(LV)}$ would be dramatically slowed to hundreds of milliseconds compared to the millisecond time scale reported in our experiments.

As a result, the outstanding question concerned possible mechanisms by which $[K^+]_c$ might affect permeation through $G_{K(LV)}$ from the outside. An initial clue was gleaned from experiments in which 5 mM of Ca^{2+}, Mg^{2+} or Ba^{2+} replaced the total 2.8 mM Ca^{2+} and 2.2 mM Mg^{2+} in the typical recording solution. The size of the initial current jump upon depolarization was in the order $Ba^{2+} > Mg^{2+} > Ca^{2+}$, suggesting that the $G_{K(LV)}$ at the holding potential could be blocked by divalent ions, with Ca^{2+} being the most potent. That led to experiments using 4 mM K^+ and 5 mM Mg^{2+} in the external solution to which EGTA had been added to selectively chelate free Ca^{2+} (Fig. 8A). Our typical 25 ms protocols revealed that $G_{K(LV)}$ was 50% open at the holding potential under these conditions, but this was not as complete a linearization of the I-V curve as observed with elevation of $[K^+]_o$ to 20 mM. The kinetics of EGTA buffering is slow (Naraghi, 1997), and the $[pH]_c$ varies over the course of hair cell depolarization (Highstein *et al.*, 2014). This suggested that lengthening the pulse duration to 500 ms might increase calcium binding and increase the instantaneous IK_{LV}. We found, with increased duration, a complete linearization of the I-V curve (Fig. 8C). We assumed that this action was on the $G_{K(LV)}$, since removal of Ca^{2+} would block activation of I_{BK} (Meech & Standen, 1975) and interfere with transduction by breaking the tip links on the stereocilia (Crawford *et al.*, 1991). The EGTA manipulation had surprisingly little effect on the I_{Ca}, which in solitary cells would strip Ca^{2+} binding within the channel and increase the amplitude by up to 3X with Na^+ and K^+ as permeant ions (Art *et al.*, 1993). So, it remains uncertain whether, in the context of the synaptic cleft, the EGTA reached the calcium channels and was rapid enough to chelate the Ca^{2+} released from synaptic vesicles (Israel *et al.*, 1980), or was transported through the basolateral surface (Boyer *et al.*, 2001). The impact of calcium removal on the adhesion molecules between the type I hair cell and its surrounding calyx (Lysakowski *et al.*, 2011) is difficult to assess, although reduction of $[Ca^{2+}]_c$ in other epithelia is known to reduce coupling, thereby potentially increasing the width of the cleft and lowering the external $[K^+]_c$.

Taken together, these results suggested that what initially appeared to be a voltage-activated potassium conductance activating at potentials depolarized from E_K (Rennie & Correia, 1994; Rusch & Eatock, 1996; Spaiardi *et al.*, 2017), might acquire its apparent voltage-sensitivity through a sensitivity to $[K^+]_c$. The source of K^+ at any potential is complex, but given the experiments from a holding potential of −100 mV, small amounts of $G_{K(LV)}$ activate at potentials hyperpolarized to the activation of G_{Ca} and G_{BK} (Fig. 1B), and thus it would be responsible for a background elevation of $[K^+]_c$ above that found in the bath. At

more depolarized potentials, as the latter two conductances are activated, $[K^+]_c$ would be rapidly elevated by K^+ flux through neighboring G_{BK}. At successively more depolarized potentials where more of the $G_{K(LV)}$ is activated, the K^+ flux represented by I_{BK} and $I_{K(LV)}$ would combine to elevate $[K^+]_c$ and unblock additional K_{LV} channels. Such a scheme would explain how generation of larger I_{BK} resulted in larger and earlier IK_{LV} (Fig. 1A, inset), as well as the reduction and slowing of IK_{LV} when I_{BK} was blocked directly with IbTX (Fig. 5) or indirectly by buffering $[Ca^{2+}]_i$ with BAPTA or blocking I_{Ca} with Compound VIII (Fig. 4).

To summarize these effects, we constructed a simple blocking model with few assumptions other than, by symmetry with inward rectification (Woodhull, 1973; Goodman & Art, 1996a), that the outward rectification was the result of a block of permeation near or in the external mouth of the channel (Eqs. 6 - 12). This block by Ca^{2+} and its relief by K^+ could be modeled as an apparent voltage-dependent block between closed and open states in which the inherent Ca^{2+} block was relieved by elevating $[K^+]_c$ as a result of voltage-dependent I_K through neighboring channels in the cleft. Such a model gave reasonable fits to the rectification in normal and elevated $[K^+]_o$ (Fig. 9C). Anatomical support for the model is based on prior on-cell patch recordings in type I hair cells (Lapeyre *et al.*, 1993) that demonstrated three types of channels present along the base of the hair cell, with large-conductance channels whose probability of opening decreased as the internal $[Ca^{2+}]_i$ was lowered were found not only on the base, but also along the neck as well. With such a distribution, the activation from a holding potential of −100 mV would activate the G_{Ca} and G_{BK} over the entire basolateral surface, thereby elevating $[K^+]_c$ throughout the cleft, naturally leading to a subsequent relief of the block of $G_{K(LV)}$.

Similarities in the gating of IK_{LV} and C-type inactivation – implications for a synapse.

Ion permeation is often regulated in a pore at both an internal gate with allosteric coupling to voltage, chemical, or mechanical force, and a selectivity filter near the external mouth that determines which ions are permitted to transit the pore. In voltage-dependent channels, the opening may be associated with subsequent inactivation associated with either the N-terminus (N-type) or C-terminus (C-type) and the outer aspect of the channel (Hoshi *et al.*, 1991). In many preparations (Baukrowitz & Yellen, 1995; Levy & Deutsch, 1996; Johnson *et al.*, 1999; Armstrong & Hoshi, 2014; Carrillo *et al.*, 2015), the rate of C-type inactivation and deactivation can be modulated, with elevated $[Ca^{2+}]_o$ increasing and elevated $[K^+]_o$ decreasing the rate of inactivation or deactivation. In some, the inactivation is sensitive to pH as well (Lesage & Barhanin, 2011). A functional theme is that K^+-sensitive modulation would allow for a dynamic adjustment of the potassium conductance and currents in response to repetitive activity that elevates $[K^+]_o$ in the intercellular space (Baukrowitz & Yellen, 1995).

The acceleration of the kinetic response and the linearization of the $G_{K(LV)}$ I-V curve when $[K^+]_c$ is elevated or $[Ca^{2+}]_c$ is reduced is consistent with a model in which an internal gate has little voltage-sensitivity, or opens at very hyperpolarized potentials, and flux through the channel is controlled by the selectivity filter switching between inactivated and activated states based on ion concentrations in the cleft. With the gate open from hyperpolarized potentials, the channel would effectively become a conductance whose value would be

determined by $[K^+]_c$ and $[Ca^{2+}]_c$. The similarity between elements of C-type inactivation and the proposed regulation of permeation through $G_{K(LV)}$ can by understood by analogy to the proposed crystal structures of the closed, open, and inactivated states of the KcsA channel (Fig. 11, modified from (Cuello *et al.*, 2017). A voltage-controlled channel at a hyperpolarized holding potential is initially in a state where the gate is closed, and when it has recovered from inactivation the selectivity filter is open, the state C/O (Fig. 11, left). With depolarization, the channel moves along path 'a', and the gate opens with K^+ free to permeate through the selectivity filter, the state O/O (Fig. 11, middle). With the channel in this configuration, under maintained depolarization, it moves along path 'b', and the selectivity filter becomes inactivated, the state O/I (Fig. 11, right). For path 'b' we have explicitly added the effects of elevating $[K^+]_o$ or $[Ca^{2+}]_o$, which would drive the channel in opposite directions toward O/O or O/I, respectively. The internal gate is open in both states, and as with our experiments, permeation is regulated by the concentrations of the permeant ion modulating the selectivity filter between inactivated and non-inactivated states, and not by the opening and closing of a voltage-sensitive gate. In short, the model would require that the gate remain open, a condition met for example with the MinK-KCNQ1 channel where a single amino acid substitution F340W-I_{Ks} decouples the gate from the voltage-sensitive domain and renders it constitutively open (Panaghie *et al.*, 2008). In our experiments, hyperpolarization below −110 mV began to show signs of rectification (Figs. 7B, 9C), suggesting that if the $G_{K(LV)}$ retains a voltage-sensitive internal gate, then it is opened at potentials hyperpolarized to the physiological range.

It should also be noted that the total outward conductance that could be elicited from a holding potential of −100 mV was 408% larger than that measured when the hair cell was held at −70 mV, indicating that 74% of the conductance had been inactivated. Given the inter-dependencies between the three conductances, inactivation could arise at any or all of them. Calmodulin supports both activation and inactivation of the L-type calcium channel (Zuhlke *et al.*, 1999), and accessory β subunits of the BK channel are the molecular basis of different forms of its inactivation (Martinez-Espinosa *et al.*, 2014). Since the voltage-dependence of activation and inactivation curves for conductances are independent, by holding cells at −70 mV it is assured that G_{Ca} and G_{BK} were below their activation voltages. However, without further experiments we can say little about the steady-state inactivation of either, or how much additional down-stream conductance, G_{BK} or $G_{K(LV)}$, could be elicited by depolarization. Based on the instantaneous currents from the −70 mV holding potential (Fig. 9B), the resting conductance of 26.7 nS (30 ± 20 nS) is 67.1% of the total of 39.8 nS (37.1 ± 19.2 nS, n = 19) that can be recruited from this potential. Since ¾th of the total outward current elicited from the −100 mV holding potential occurred through the $G_{K(LV)}$ (Figs. 1C, 2), and it was this conductance that was sensitive to $[K^+]_o$ and $[Ca^{2+}]_o$, we assume that it is much of this conductance that is inactivated, either directly and/or additionally by inactivation of upstream currents.

Regulation of potassium conductances such as $G_{K(LV)}$ by $[K^+]_c$, and perhaps other ions, has a number of functional advantages in the context of the synaptic cleft between hair cell and afferent where $[H^+]_c$, $[Ca^{2+}]_c$, and $[K^+]_c$ would all change dynamically during ongoing activity. For synaptic transmission to occur, a standing transduction current, in addition to any other inward cation currents, depolarizes the hair cell. An historic concern was that

transduction currents exiting across a high basolateral conductance would not be sufficient to depolarize the cell to potentials where I_{Ca} would be activated (Chen, 1995; Lim *et al.*, 2011; Contini *et al.*, 2012). That assumption was based on the apparent hyperpolarized activation of $G_{K(LV)}$, with an associated large conductance on at nominal resting potentials. With a fixed E_K and driving force through this conductance, large transduction currents would be needed to depolarize the hair cell by even a few mV, much less to potentials necessary for activation of the G_{Ca}. When held at −100 mV, the 25 ms depolarizations and chord conductance measurements (Fig. 1) demonstrated that $G_{K(LV)}$ did not increase significantly until the cell was depolarized above potentials needed to activate I_{Ca} and I_{BK} and the $[K^+]_c$ was in excess of 6 – 8 mM. If true, then depolarizing transduction currents would actually flow across a relatively low basolateral conductance until reaching the depolarized potentials where I_{Ca} and I_{BK} are activated. At this potential, the positive feedback of I_{Ca} effectively assists in depolarizing the hair cell, and I_{BK} and the IK_{LV} serve as negative feedback tending to hyperpolarize the cell. As $[K^+]_c$ increases, however, the E_K depolarizes, reducing the negative feedback due to I_{BK} and IK_{LV} that allows the hair cell to depolarize to a new zero-current potential at a potential a few mV above the new E_K. For type I hair cells with functional transduction channels bathed in low-calcium, high-potassium endolymph and an intact enveloping synaptic cleft, this may be considerably depolarized with respect to the values currently quoted for solitary cells in high-calcium, high-sodium artificial perilymph. Clearly the steady-state $[K^+]_c$ would depend not only on the presynaptic hair cell, but on influx into the afferent through its conductances (Lysakowski *et al.*, 2011) and transporters (Schuth *et al.*, 2014), as well as diffusion out from the apical gap between the two. In a synaptic context, $G_{K(LV)}$ is designed to be exquisitely modulated by the local changes in ion concentration. Based on shaker inactivation, for example, elevation of $[K^+]_c$ by any pre- or postsynaptic source would positively feedback on $G_{K(LV)}$ and increase its conductance, while elevations of either $[H^+]_c$ or $[Ca^{2+}]_c$ associated with synaptic quanta or basolateral hair cell transporters would negatively feedback on $G_{K(LV)}$ and reduce it.

Functional implications of two conductances contributing to the modulation of $[K^+]_c$

Most prior studies used solitary cells isolated from unspecified locations within an epithelium, and presented data in which a major outward current could be blocked by 4-AP (Rennie & Ashmore, 1991; Rusch & Eatock, 1996). Since 4-AP blocks a broad spectrum of potassium conductances, in the absence of dose-response relationships and the relative blocking affinities for the currents in these studies, we are unable to assess the extent to which currents remaining with a single dose represent the residual of a single current, or another current with a distinct k_i. Given the interdependencies of the conductances revealed in our study, the precise blocking order might also be impactful.

We have restricted our analysis to the central region of the vestibular epithelium where the calyceal and dimorphic afferent response dynamics to natural stimuli are known to be more phasic than those from afferents innervating the surrounding epithelium (Brichta & Goldberg, 2000). In response to a maintained step of inward current, either through transduction channels or by injection through the recording electrode, type I hair cells have a voltage response in which peak depolarization is followed by relaxation to less depolarized

potentials (Contini *et al.*, 2017). Such adaptation in membrane potential requires that the basolateral conductance and outward current on at rest are less than that achieved toward the end of the step. Viewed in terms of currents, it requires that an inward transduction current initially dominate and drive the potential to its peak, and over time the outward current would need to increase monotonically in order to repolarize the membrane to lower potentials. In the context of a synaptic cleft, minimizing adaptation of the outward current would require – in the face of increasing $[K^+]_c$ - a contemporaneous increase in potassium conductance, G_K, that compensates for the decreased driving force resulting from the elevated $[K^+]_c$.

The proportional expression of the G_{BK} and the $G_{K(LV)}$ also carries functional implications. A high proportion of G_{BK} in a hair cell would result in rapid elevation of $[K^+]_c$ and larger and more rapid activation of the associated $G_{K(LV)}$. Viewed in current clamp, in response to a constant step of transducer current, the membrane potential would peak and rapidly decay to much lower potentials. The membrane potential response would effectively differentiate the input current. As the amount of G_{BK} is reduced compared to the expression of $G_{K(LV)}$, the rate of adaptation in membrane potential would be slowed, and the decay would be to less hyperpolarized potentials. In short, the response in the latter case would be more tonic, and more faithfully following the depolarizing current. The variations in total conductance (Fig. 1D) and fractions of G_{BK} and $G_{K(LV)}$ in the population as determined by 4-AP^+ block (Fig. 2F), revealed appreciable variations in expression of each conductance. Functionally, such variation would naturally contribute to a range of dynamic response properties and signaling of distinct types of head movement.

Modes of synaptic transmission: quantal, ion accumulation, and resistive coupling

The standard models of synaptic transmission reflect the dominance of quantal (Katz, 1969), and to a lesser extent electrical transmission (Furshpan & Potter, 1959) in the vertebrate and invertebrate nervous systems. Chemical transmission is frequently complex, with quantal co-transmission of multiple fast transmitters (Jonas *et al.*, 1998), or fast transmission augmented by slower peptide modulators (Jan *et al.*, 1979), often with the release of the latter determined by the pattern of presynaptic activity (Whim & Lloyd, 1994). Occasionally, chemical and electrical transmission are combined, such as in the chick ciliary ganglion (Martin & Pilar, 1963), and both orthodromic and antidromic transmission resulting from the electrical coupling can be demonstrated experimentally. In non-spiking neurons - particularly those with slow changes in potential such as cells in outer retina, alternatives to quantal and electrical transmission incorporating ion- and voltage-dependent reversal of transmitter transporters have been proposed (Schwartz, 2002).

Calyceal afferents receive quantal input from type I hair cells synapsing on the inner face of the calyx, and type II hair cells synapsing onto the outer face (Lysakowski & Goldberg, 1997). With fluid stimulation of the mechano-electrical transducer, MET, in turtle, rates of quantal release could exceed 1000 s^{-1} and EPSCs ranged in amplitude from < 8 to > 400 pA (Highstein *et al.*, 2015; Contini *et al.*, 2017). The latter study also suggested that the largest EPSCs originate from the type II hair cells synapsing on the outer face of the calyx. In parallel with quantal transmission are signs of the more exotic modes of synaptic

transmission proposed in the retina, such as ion accumulation in the cleft. Optical (Highstein *et al.*, 2014) and electrophysiological (Contini *et al.*, 2017) experiments measured changes in $[H^+]_c$ and $[K^+]_c$ associated with hair cell depolarization. In our dual-recordings, we concluded that transmission by quantal release and ion accumulation are multiplexed in parallel across the synaptic pair, since quantal transmission was observed in all cases in which the hair cell was depolarized above the threshold for calcium entry. Accumulation of K^+ and H^+ were antagonistic in the cleft. Elevation of $[K^+]_c$ depolarized both hair cell and afferent, regardless of the source of potassium efflux into the cleft, but elevation of $[H^+]_c$ decreased all three hair cell conductances, and reduced the induced inward current through the afferent HCN conductance, as could be demonstrated by increased pH buffering in the cleft (Contini *et al.*, 2017).

The main conclusion from the previous study was that the potassium flux out of the large basolateral potassium conductance was sufficient to elevate $[K^+]_c$ and depolarize its reversal potential, resulting in hair cell depolarization to potentials where calcium influx drove quantal transmission (Fig. 12A). In the absence of the restricted extracellular space, inward transduction current would flow out the basolateral conductance and fail to depolarize the cell. Depolarization of either hair cell or afferent would result in $[K^+]_c$ elevation. Other non-traditional modes such as electrical and ephaptic transmission are considered less likely at this synapse. Electrical resistive coupling between hair cell and afferent was not observed when ion conductances were blocked, and there was no anatomical evidence for gap junctions between the two cells (Gulley & Bagger-Sjöbäck, 1979). The possibility of ephaptic transmission in an intact preparation was difficult to assess. In the reduced preparation of our experiments, the access resistance is the pipette series resistance added to the parallel sum of all paths from the cell interior to ground. A large impedance necessary for this form of transmission (Katz & Schmitt, 1940) was not found, although it might have been compromised by low impedance paths not present if the apical tight junction of the epithelium were intact.

However, in two types of protocols an interesting coupling between hair cell and afferent was observed that relies on the large hair cell and afferent conductances on at their resting potentials. At these potentials, rapid depolarizations that appear to be attenuated APs antidromically propagated from the spike initiation site into the afferent were associated with phase-locked hair cell potentials of similar form but 20 – 25% of the amplitude of the afferent potentials (Fig. 2A, (Contini *et al.*, 2017)). A more direct observation of such resistive coupling could be demonstrated with both cells held in voltage clamp. As noted in Results, at a holding potential of −70 mV (Fig. 10B, C), for 2 nA of outward hair cell current, ~25 pA of rapid inward current flowed into the afferent (Fig. 10C). By Kirchhoff's current law, apical inward transduction current flows out through the basolateral hair cell membrane as I_K, and will divide to flow along the cleft and out into the bath, or directly into the surrounding afferent (Fig. 12B). As $[K^+]_c$ increases and the potassium and mixed conductances of the afferent increase, fractionally more of this transduction current will be diverted into the afferent. By this means, the modulation of the resting hair cell and afferent conductance serves as a dynamic way of controlling the resistive coupling between the two cells. Though dependent on the precise resting potentials of the two, in general the larger the G_K and G_{HCN} on the inner face of the afferent on at rest, the larger the fraction of transducer

current flowing out of the hair cell that will flow into the calyx as $[K^+]_c$ is elevated. Unlike conventional electrical transmission via connexins (Bennett, 1997), which can be modulated by $[H^+]_i$ and $[Ca^{2+}]_i$ (Obaid *et al.*, 1983), this would provide not only rapid, bidirectional communication between cells, but the degree of coupling itself would be modified by ongoing activity of either cell and the resulting instantaneous $[K^+]_c$.

Our conclusion is that at the type I hair cell – afferent synapse there are three modes of communication that range from tens of milliseconds to tens of microseconds. The slowest mode of transmission is the potassium ion accumulation in the cleft that serves as a bidirectional mechanism by which both hair cell and afferent are depolarized to potentials that allow rapid vesicle fusion and the potential for EPSPs to trigger APs. Given the volume of the cleft, our estimates are that changes in ion concentration occur over the course of tens of milliseconds and reflect a relatively low-pass filtering of recent activity. The second more intermediate speed of transmission with millisecond packets of transmitter is conventional glutamatergic quantal transmission that was observed in all cases where the hair cell was depolarized to potentials necessary for calcium influx and vesicle fusion. With the afferent resting at potentials slightly hyperpolarized to that necessary for AP generation, information would be rapidly and faithfully communicated across the synapse if the first quantum released by depolarization generates an AP in the afferent (Curthoys *et al.*, 2018). The unexpected third form of synaptic transmission is the most rapid, and results from the large basolateral hair cell conductances and the inner-face calyx conductances that are on at their resting potentials. Like ion accumulation, this is bidirectional transmission, and a current flowing out of either hair cell or afferent at the synapse will divide between a fraction flowing in the intercellular cleft and out into the bath, and a fraction flowing across the cleft into its cellular partner. This mode of transmission potentially may occur within tens of microseconds since current division requires no changes in cellular potential, and the amplitude of the dynamic coupling between the hair cell $G_{K(LV)}$ and the afferent G_{HCN} would be greatest under conditions that elevate $[K^+]_c$ the most.

Acknowledgments

Funding:

Funded by U.S. HHS, NIH, National Institute on Deafness and Other Communication Disorders, grants R01 DC002058, R01 DC008846, R21 DC016454 R21 DC017292; R21 DC017577.

The work was performed in his laboratory and used the common core microscopy facilities, financial, and administrative support of the Department of Anatomy & Cell Biology. All authors have approved the final version of the manuscript, agree to be accountable for all aspects of the work, and qualify for authorship. All those who qualify for authorship are listed.

Abbreviations list:

4-AP	4-Aminopyridine, $C_5H_4N–NH_2$
4-AP$^+$	4-Aminopyridinium, C_5H_5N-NH_2
AAALAC	Association for the Assessment and Accreditation of Laboratory Animal Care

ALEXA Fluor 488	fluorescent dye with maxima (in nm) of 495 abs, 519 em.
ALEXA Fluor 568	fluorescent dye with maxima of 568 abs, 603 em.
BAPTA	1,2-*bis*(*o*-Aminophenoxy)ethane-N,N,N′,N′-tetraacetic Acid, 4K-salt
BK	large calcium-activated potassium channel, $K_{Ca}1.1$
$Ca_V1.3$	calcium channel, voltage-dependent, L-type, alpha 1D subunit
Compound VIII	1-(3-Chlorophenethyl)-3-cyclopentylpyrimidine-2,4,6-(1H, 3H,5H)-trione
$C_{17}H_{19}CIN_2O_3$	PubChem CID: 57520395, SID:170474596
$[X]_{c,i,o}$	concentration of ion X in the synaptic *c*left, *i*ntracellular solution, or *o*utside bath
G_{BK}	large calcium-activated potassium conductance
G_{Ca}	calcium conductance
$G_{K(LV)}$	low-voltage activating potassium conductance
HCN	hyperpolarization-activated cyclic nucleotide-gated channel
IACUC	Institutional Animal Care and Use Committee
IbTX	Iberiotoxin
I_K	Potassium current
$I_{K(Ca)}$	large calcium-activated potassium current
$I_{K(LV)}$	low-voltage-activated potassium current
K_{LV}	low-voltage-activated channel
MET	mechano-electrical transducer
TEA-Cl	Tetraethylamonium-Chloride
ZD7288	an HCN channel blocker

References

Armstrong CM. (1969). Inactivation of the potassium conductance and related phenomena caused by quaternary ammonium ion injection in squid axons. J Gen Physiol 54, 553–575. [PubMed: 5346528]

Armstrong CM & Bezanilla F. (1977). Inactivation of the sodium channel. II. Gating current experiments. J Gen Physiol 70, 567–590. [PubMed: 591912]

Armstrong CM & Hoshi T. (2014). K^+ channel gating: C-type inactivation is enhanced by calcium or lanthanum outside. J Gen Physiol 144, 221–230. doi:10.1085/jgp.201411223 [PubMed: 25156116]

Art JJ & Fettiplace R. (1987). Variation of membrane properties in hair cells isolated from the turtle cochlea. J Physiol 385, 207–242. [PubMed: 2443666]

Art JJ, Fettiplace R & Wu YC. (1993). The effects of low calcium on the voltage-dependent conductances involved in tuning of turtle hair cells. J Physiol 470, 109–126. [PubMed: 8308720]

Art JJ, Wu YC & Fettiplace R. (1995). The calcium-activated potassium channels of turtle hair cells. J Gen Physiol 105, 49–72. [PubMed: 7730789]

Bao H, Wong WH, Goldberg JM & Eatock RA. (2003). Voltage-gated calcium channel currents in type I and type II hair cells isolated from the rat crista. J Neurophysiol 90, 155–164. doi:10.1152/jn.00244.2003 [PubMed: 12843307]

Baukrowitz T & Yellen G. (1995). Modulation of K^+ current by frequency and external [K^+]: a tale of two inactivation mechanisms. Neuron 15, 951–960. [PubMed: 7576643]

Bennett MVL. (1997). Gap junctions as electrical synapses. J Neurocytol 26, 349–366. doi:Doi 10.1023/A:1018560803261 [PubMed: 9278865]

Blatz AL & Magleby KL. (1986). Quantitative description of three modes of activity of fast chloride channels from rat skeletal muscle. J Physiol 378, 141–174. [PubMed: 2432249]

Boyer C, Art JJ, Dechesne CJ, Lehouelleur J, Vautrin J & Sans A. (2001). Contribution of the plasmalemma to Ca^{2+} homeostasis in hair cells. J Neurosci 21, 2640–2650. [PubMed: 11306617]

Brelidze TI & Magleby KL. (2004). Protons block BK channels by competitive inhibition with K^+ and contribute to the limits of unitary currents at high voltages. J Gen Physiol 123, 305–319. doi:10.1085/jgp.200308951 [PubMed: 14981139]

Brichta AM, Aubert A, Eatock RA & Goldberg JM. (2002). Regional analysis of whole cell currents from hair cells of the turtle posterior crista. J Neurophysiol 88, 3259–3278. doi:10.1152/jn.00770.2001 [PubMed: 12466445]

Brichta AM & Goldberg JM. (2000). Morphological identification of physiologically characterized afferents innervating the turtle posterior crista. J Neurophysiol 83, 1202–1223. [PubMed: 10712450]

Candia S, Garcia ML & Latorre R. (1992). Mode of action of iberiotoxin, a potent blocker of the large conductance Ca^{2+}-activated K^+ channel. Biophys J 63, 583–590. doi:10.1016/S0006-3495(92)81630-2 [PubMed: 1384740]

Carrillo E, Pacheco L, Balleza D & Gomez-Lagunas F. (2015). K^+-dependent selectivity and external Ca^{2+} block of Shab K^+ channels. PLoS One 10, e0120431. doi:10.1371/journal.pone.0120431

Chen JW & Eatock RA. (2000). Major potassium conductance in type I hair cells from rat semicircular canals: characterization and modulation by nitric oxide. J Neurophysiol 84, 139–151. [PubMed: 10899192]

Chen W-Y. (1995). The Properties and Functions of a Low-Voltage Activated K1 Current in Type I Hair Cells of Rat Semicircular Canal Organs. (Ph.D. Dissertation), University of Rochester, Rochester, NY.

Cho S & von Gersdorff H. (2014). Proton-mediated block of Ca^{2+} channels during multivesicular release regulates short-term plasticity at an auditory hair cell synapse. J Neurosci 34, 15877–15887. doi:10.1523/JNEUROSCI.2304-14.2014 [PubMed: 25429130]

Contini D, Price SD & Art JJ. (2017). Accumulation of K^+ in the synaptic cleft modulates activity by influencing both vestibular hair cell and calyx afferent in the turtle. J Physiol 595, 777–803. doi:10.1113/JP273060 [PubMed: 27633787]

Contini D, Zampini V, Tavazzani E, Magistretti J, Russo G, Prigioni I & Masetto S. (2012). Intercellular K^+ accumulation depolarizes Type I vestibular hair cells and their associated afferent nerve calyx. Neuroscience 227, 232–246. doi:10.1016/j.neuroscience.2012.09.051 [PubMed: 23032932]

Crawford AC, Evans MG & Fettiplace R. (1991). The actions of calcium on the mechano-electrical transducer current of turtle hair cells. J Physiol 434, 369–398. [PubMed: 1708822]

Crawford AC & Fettiplace R. (1980). The frequency selectivity of auditory nerve fibres and hair cells in the cochlea of the turtle. J Physiol 306, 79–125. [PubMed: 7463380]

Cruz-Rangel S, De Jesus-Perez JJ, Contreras-Vite JA, Perez-Cornejo P, Hartzell HC & Arreola J. (2015). Gating modes of calcium-activated chloride channels TMEM16A and TMEM16B. J Physiol 593, 5283–5298. doi:10.1113/JP271256 [PubMed: 26728431]

Cuello LG, Cortes DM & Perozo E. (2017). The gating cycle of a K+ channel at atomic resolution. Elife 6. doi:10.7554/eLife.28032

Cuello LG, Jogini V, Cortes DM & Perozo E. (2010). Structural mechanism of C-type inactivation in K $^{+}$ channels. Nature 466, 203–208. doi:10.1038/nature09153 [PubMed: 20613835]

Curthoys IS, Burgess AM & Goonetilleke SC. (2018). Phase-locking of irregular guinea pig primary vestibular afferents to high frequency (>250Hz) sound and vibration. Hear Res 373, 59–70. doi: 10.1016/j.heares.2018.12.009 [PubMed: 30599427]

Curtis HJ & Cole KS. (1942). Membrane resting and action potentials from the squid giant axon. J Cell Comp Physiol 19, 135–144. doi:10.1002/jcp.1030190202

DeVries SH. (2001). Exocytosed protons feedback to suppress the Ca^{2+} current in mammalian cone photoreceptors. Neuron 32, 1107–1117. [PubMed: 11754841]

DeVries SH, Qi X, Smith R, Makous W & Sterling P. (2002). Electrical coupling between mammalian cones. Curr Biol 12, 1900–1907. [PubMed: 12445382]

Eatock RA & Hutzler MJ. (1992). Ionic currents of mammalian vestibular hair cells. Ann N Y Acad Sci 656, 58–74. [PubMed: 1376099]

Forsythe ID. (1994). Direct patch recording from identified presynaptic terminals mediating glutamatergic EPSCs in the rat CNS, in vitro. J Physiol 479 (Pt 3), 381–387. [PubMed: 7837096]

Fuchs PA, Evans MG & Murrow BW. (1990). Calcium currents in hair cells isolated from the cochlea of the chick. J Physiol 429, 553–568. [PubMed: 1703574]

Furshpan EJ & Potter DD. (1959). Transmission at the giant motor synapses of the crayfish. J Physiol 145, 289–325. [PubMed: 13642302]

Galvez A, Gimenez-Gallego G, Reuben JP, Roy-Contancin L, Feigenbaum P, Kaczorowski GJ & Garcia ML. (1990). Purification and characterization of a unique, potent, peptidyl probe for the high conductance calcium-activated potassium channel from venom of the scorpion Buthus tamulus. J Biol Chem 265, 11083–11090. [PubMed: 1694175]

Geng Y, Wang X & Magleby KL. (2013). Lack of negative slope in I-V plots for BK channels at positive potentials in the absence of intracellular blockers. J Gen Physiol 141, 493–497. doi: 10.1085/jgp.201210955 [PubMed: 23530138]

Goldman DE. (1943). Potential, Impedance, and Rectification in Membranes. J Gen Physiol 27, 37–60. doi:10.1085/jgp.27.1.37 [PubMed: 19873371]

Gomez-Lagunas F, Melishchuk A & Armstrong CM. (2003). Block of Shaker potassium channels by external calcium ions. Proc Natl Acad Sci U S A 100, 347–351. doi:10.1073/pnas.0237122100 [PubMed: 12509504]

Goodman MB & Art JJ. (1996a). Positive feedback by a potassium-selective inward rectifier enhances tuning in vertebrate hair cells. Biophys J 71, 430–442. doi:10.1016/s0006-3495(96)79245-7 [PubMed: 8804626]

Goodman MB & Art JJ. (1996b). Variations in the ensemble of potassium currents underlying resonance in turtle hair cells. J Physiol 497 (Pt 2), 395–412. [PubMed: 8961183]

Green GE, Khan KM, Beisel DW, Drescher MJ, Hatfield JS & Drescher DG. (1996). Calcium channel subunits in the mouse cochlea. J Neurochem 67, 37–45. [PubMed: 8667015]

Grissmer S & Cahalan M. (1989). TEA prevents inactivation while blocking open K^{+} channels in human T lymphocytes. Biophys J 55, 203–206. doi:10.1016/S0006-3495(89)82793-6 [PubMed: 2784693]

Gulley RL & Bagger-Sjöbäck D. (1979). Freeze-fracture studies on the synapse between the type I hair cell and the calyceal terminal in the guinea-pig vestibular system. J Neurocytol 8, 591–603. [PubMed: 317909]

Haynes LW, Kay AR & Yau KW. (1986). Single cyclic GMP-activated channel activity in excised patches of rod outer segment membrane. Nature 321, 66–70. doi:10.1038/321066a0 [PubMed: 2422558]

Held H. (1893). Die centrale Gehörleitung. Archiv für Anatomie und Physiologie Anatomische Abteilung 17, 201–248.

Hess P, Lansman JB & Tsien RW. (1986). Calcium channel selectivity for divalent and monovalent cations. Voltage and concentration dependence of single channel current in ventricular heart cells. J Gen Physiol 88, 293–319. [PubMed: 2428919]

Highstein SM, Holstein GR, Mann MA & Rabbitt RD. (2014). Evidence that protons act as neurotransmitters at vestibular hair cell-calyx afferent synapses. Proc Natl Acad Sci U S A 111, 5421–5426. doi:10.1073/pnas.1319561111 [PubMed: 24706862]

Highstein SM, Mann MA, Holstein GR & Rabbitt RD. (2015). The quantal component of synaptic transmission from sensory hair cells to the vestibular calyx. J Neurophysiol 113, 3827–3835. doi: 10.1152/jn.00055.2015 [PubMed: 25878150]

Hladky SB & Haydon DA. (1972). Ion transfer across lipid membranes in the presence of gramicidin A. I. Studies of the unit conductance channel. Biochim Biophys Acta 274, 294–312. [PubMed: 5048999]

Hodgkin AL & Horowicz P. (1959). The influence of potassium and chloride ions on the membrane potential of single muscle fibres. J Physiol 148, 127–160. [PubMed: 14402240]

Hodgkin AL & Katz B. (1949). The effect of sodium ions on the electrical activity of giant axon of the squid. J Physiol 108, 37–77. doi:10.1113/jphysiol.1949.sp004310 [PubMed: 18128147]

Horie M, Irisawa H & Noma A. (1987). Voltage-dependent magnesium block of adenosine-trisphosphate-sensitive potassium channel in guinea-pig ventricular cells. J Physiol 387, 251–272. [PubMed: 2443681]

Horwitz GC, Risner-Janiczek JR, Jones SM & Holt JR. (2011). HCN channels expressed in the inner ear are necessary for normal balance function. J Neurosci 31, 16814–16825. doi:10.1523/JNEUROSCI.3064-11.2011 [PubMed: 22090507]

Hoshi T & Armstrong CM. (2013). C-type inactivation of voltage-gated K^+ channels: pore constriction or dilation? J Gen Physiol 141, 151–160. doi:10.1085/jgp.201210888 [PubMed: 23319730]

Hoshi T, Zagotta WN & Aldrich RW. (1991). Two types of inactivation in Shaker K^+ channels: effects of alterations in the carboxy-terminal region. Neuron 7, 547–556. [PubMed: 1931050]

Huang H, Ng CY, Yu D, Zhai J, Lam Y & Soong TW. (2014). Modest CaV1.342-selective inhibition by compound 8 is beta-subunit dependent. Nat Commun 5, 4481. doi:10.1038/ncomms5481 [PubMed: 25057870]

Hudspeth AJ & Lewis RS. (1988). Kinetic analysis of voltage- and ion-dependent conductances in saccular hair cells of the bull-frog, Rana catesbeiana. J Physiol 400, 237–274. [PubMed: 2458454]

Immke DC & McCleskey EW. (2003). Protons open acid-sensing ion channels by catalyzing relief of Ca^{2+} blockade. Neuron 37, 75–84. [PubMed: 12526774]

Israel M, Manaranche R, Marsal J, Meunier FM, Morel N, Frachon P & Lesbats B. (1980). ATP-dependent calcium uptake by cholinergic synaptic vesicles isolated from Torpedo electric organ. J Membr Biol 54, 115–126. [PubMed: 7401165]

Jan YN, Jan LY & Kuffler SW. (1979). A peptide as a possible transmitter in sympathetic ganglia of the frog. Proc Natl Acad Sci U S A 76, 1501–1505. [PubMed: 35789]

Johnson JP Jr., Mullins FM & Bennett PB. (1999). Human ether-a-go-go-related gene K^+ channel gating probed with extracellular Ca^{2+}. Evidence for two distinct voltage sensors. J Gen Physiol 113, 565–580. [PubMed: 10102937]

Jonas P, Bischofberger J & Sandkuhler J. (1998). Corelease of two fast neurotransmitters at a central synapse. Science 281, 419–424. [PubMed: 9665886]

Kang S, Cooper G, Dunne SF, Dusel B, Luan CH, Surmeier DJ & Silverman RB. (2012). CaV1.3-selective L-type calcium channel antagonists as potential new therapeutics for Parkinson's disease. Nat Commun 3, 1146. doi:10.1038/ncomms2149 [PubMed: 23093183]

Katz B. (1969). The Sherrington Lectures The release of neural transmitter substances, vol. 10 Liverpool University Press.

Katz B & Schmitt OH. (1940). Electric interaction between two adjacent nerve fibres. J Physiol 97, 471–488. doi:10.1113/jphysiol.1940.sp003823 [PubMed: 16995178]

Kim JG, Park SW, Shin KC, Kim B, Byun D & Bae YM. (2019). Measurement of Ion Concentration in the Unstirred Boundary Layer with Open Patch-Clamp Pipette: Implications in Control of Ion Channels by Fluid Flow. J Vis Exp. doi:10.3791/58228

Kirsch GE & Narahashi T. (1983). Site of action and active form of aminopyridines in squid axon membranes. J Pharmacol and Exp Therapeutics 226, 174–179.

Kratochvil HT, Maj M, Matulef K, Annen AW, Ostmeyer J, Perozo E, Roux B, Valiyaveetil FI & Zanni MT. (2017). Probing the Effects of Gating on the Ion Occupancy of the K^+ Channel Selectivity

Filter Using Two-Dimensional Infrared Spectroscopy. J Am Chem Soc 139, 8837–8845. doi: 10.1021/jacs.7b01594 [PubMed: 28472884]

Kros CJ & Crawford AC. (1990). Potassium currents in inner hair cells isolated from the guinea-pig cochlea. J Physiol 421, 263–291. [PubMed: 2348394]

Lapeyre PN, Kolston PJ & Ashmore JF. (1993). GABAB-mediated modulation of ionic conductances in type I hair cells isolated from guinea-pig semicircular canals. Brain Res 609, 269–276. [PubMed: 7685230]

Larsen BR, Stoica A & MacAulay N. (2019). Developmental maturation of activity-induced K^+ and pH transients and the associated extracellular space dynamics in the rat hippocampus. J Physiol 597, 583–597. doi:10.1113/JP276768 [PubMed: 30357826]

Latorre R, Vergara C & Hidalgo C. (1982). Reconstitution in planar lipid bilayers of a Ca^{2+}-dependent K^+ channel from transverse tubule membranes isolated from rabbit skeletal muscle. Proc Natl Acad Sci U S A 79, 805–809. [PubMed: 6278496]

Lesage F & Barhanin J. (2011). Molecular physiology of pH-sensitive background K_{2P} channels. Physiology (Bethesda) 26, 424–437. doi:10.1152/physiol.00029.2011 [PubMed: 22170960]

Levy DI & Deutsch C. (1996). Recovery from C-type inactivation is modulated by extracellular potassium. Biophys J 70, 798–805. doi:10.1016/S0006-3495(96)79619-4 [PubMed: 8789096]

Lewis RS & Hudspeth AJ. (1983). Voltage- and ion-dependent conductances in solitary vertebrate hair cells. Nature 304, 538–541. [PubMed: 6603579]

Lim R, Kindig AE, Donne SW, Callister RJ & Brichta AM. (2011). Potassium accumulation between type I hair cells and calyx terminals in mouse crista. Exp Brain Res 210, 607–621. doi:10.1007/s00221-011-2592-4 [PubMed: 21350807]

Lopatin AN, Makhina EN & Nichols CG. (1994). Potassium channel block by cytoplasmic polyamines as the mechanism of intrinsic rectification. Nature 366, 366–369.

Lysakowski A, Gaboyard-Niay S, Calin-Jageman I, Chatlani S, Price SD & Eatock RA. (2011). Molecular microdomains in a sensory terminal, the vestibular calyx ending. J Neurosci 31, 10101–10114. doi:10.1523/jneurosci.0521-11.2011 [PubMed: 21734302]

Lysakowski A & Goldberg JM. (1997). A regional ultrastructural analysis of the cellular and synaptic architecture in the chinchilla cristae ampullares. J Comp Neurol 389, 419–443. [PubMed: 9414004]

Marchand P & Marmet L. (1983). Binomial Smoothing Filter - a Way to Avoid Some Pitfalls of Least-Squares Polynomial Smoothing. Rev Sci Inst 54, 1034–1041. doi:Doi 10.1063/1.1137498

Martin AR & Pilar G. (1963). Dual Mode of Synaptic Transmission in the Avian Ciliary Ganglion. J Physiol 168, 443–463. [PubMed: 14062687]

Martinez-Espinosa PL, Yang C, Gonzalez-Perez V, Xia XM & Lingle CJ. (2014). Knockout of the BK β2 subunit abolishes inactivation of BK currents in mouse adrenal chromaffin cells and results in slow-wave burst activity. J Gen Physiol 144, 275–295. doi:10.1085/jgp.201411253 [PubMed: 25267913]

Marty A. (1981). Ca-dependent K channels with large unitary conductance in chromaffin cell membranes. Nature 291, 497–500. [PubMed: 6262657]

Matsuda H, Saigusa A & Irisawa H. (1987). Ohmic conductance through the inwardly rectifying K channel and blocking by internal Mg^{2+}. Nature 325, 156–159. doi:10.1038/325156a0 [PubMed: 2433601]

Mayer ML & Westbrook GL. (1987). Permeation and block of N-methyl-D-aspartic acid receptor channels by divalent cations in mouse cultured central neurones. J Physiol 394, 501–527. [PubMed: 2451020]

McManus OB & Magleby KL. (1988). Kinetic states and modes of single large-conductance calcium-activated potassium channels in cultured rat skeletal muscle. J Physiol 402, 79–120. [PubMed: 3236256]

Meech RW & Standen NB. (1975). Potassium activation in Helix aspersa neurones under voltage clamp: a component mediated by calcium influx. J Physiol 249, 211–239. [PubMed: 1177091]

Meredith FL, Benke TA & Rennie KJ. (2012). Hyperpolarization-activated current (Ih) in vestibular calyx terminals: characterization and role in shaping postsynaptic events. J Assoc Res Otolaryngol 13, 745–758. doi:10.1007/s10162-012-0342-3 [PubMed: 22825486]

Meredith FL & Rennie KJ. (2016). Channeling your inner ear potassium: K^+ channels in vestibular hair cells. Hear Res. doi:10.1016/j.heares.2016.01.015

Moravec W, Peterson E & Eatock RA. (2006). Voltage-gated currents in hair cells of the turtle utricular macula. Assoc Res Otolaryngol Abs: 152.

Naraghi M. (1997). T-jump study of calcium binding kinetics of calcium chelators. Cell Calcium 22, 255–268. [PubMed: 9481476]

Nelson MT. (1986). Interactions of divalent cations with single calcium channels from rat brain synaptosomes. J Gen Physiol 87, 201–222. [PubMed: 2419482]

Obaid AL, Socolar SJ & Rose B. (1983). Cell-to-cell channels with two independently regulated gates in series: analysis of junctional conductance modulation by membrane potential, calcium, and pH. J Membr Biol 73, 69–89. [PubMed: 6306241]

Ohmori H. (1984). Studies of ionic currents in the isolated vestibular hair cell of the chick. J Physiol 350, 561–581. [PubMed: 6086899]

Panaghie G, Purtell K, Tai KK & Abbott GW. (2008). Voltage-dependent C-type inactivation in a constitutively open K^+ channel. Biophys J 95, 2759–2778. doi:10.1529/biophysj.108.133678 [PubMed: 18567635]

Press WH, Teukolsky SA, Vetterline WT & Flannery BP. (1992). Numerical recipes in C. Cambridge University Press, Cambridge, England.

Rennie KJ & Ashmore JF. (1991). Ionic currents in isolated vestibular hair cells from the guinea-pig crista ampullaris. Hear Res 51, 279–292. [PubMed: 2032962]

Rennie KJ & Correia MJ. (1994). Potassium currents in mammalian and avain isolated type I semicircular canal hair cells. J Neurophysiol 71, 317–329. [PubMed: 8158233]

Rennie KJ & Correia MJ. (2000). Effects of cationic substitutions on delayed rectifier current in type I vestibular hair cells. J Membr Biol 173, 139–148. [PubMed: 10630929]

Retzius G. (1884). Das Gehörorgan der Wirbelthiere : morphologisch-histologische Studien / Das Gehörorgan der Reptilien, der Vögel und der Säugethiere., vol. 2 Gedruckt in der Centraldruckerei : In Commission bei Samson & Wallin, Stockholm.

Roberts WM. (1993). Spatial calcium buffering in saccular hair cells. Nature 363, 74–76. [PubMed: 8479539]

Root MJ & MacKinnon R. (1994). Two identical noninteracting sites in an ion channel revealed by proton transfer. Science 265, 1852–1856. [PubMed: 7522344]

Rothman JS & Silver RA. (2018). NeuroMatic: An Integrated Open-Source Software Toolkit for Acquisition, Analysis and Simulation of Electrophysiological Data. Front Neuroinform 12, 14. doi:10.3389/fninf.2018.00014 [PubMed: 29670519]

Rusch A & Eatock RA. (1996). A delayed rectifier conductance in type I hair cells of the mouse utricle. J Neurophysiol 76, 995–1004. [PubMed: 8871214]

Salt AN, Inamura N, Thalmann R & Vora A. (1989). Calcium gradients in inner ear endolymph. Am J Otolaryngol 10, 371–375. [PubMed: 2596623]

Schnee ME & Ricci AJ. (2003). Biophysical and pharmacological characterization of voltage-gated calcium currents in turtle auditory hair cells. J Physiol 549, 697–717. doi:10.1113/jphysiol.2002.037481 [PubMed: 12740421]

Schuth O, McLean WJ, Eatock RA & Pyott SJ. (2014). Distribution of Na,K-ATPase α subunits in rat vestibular sensory epithelia. J Assoc Res Otolaryngol 15, 739–754. doi:10.1007/s10162-014-0479-3 [PubMed: 25091536]

Schwartz EA. (2002). Transport-mediated synapses in the retina. Physiol Rev 82, 875–891. doi:10.1152/physrev.00010.2002 [PubMed: 12270946]

Špaček J. (1985). Three-dimensional analysis of dendritic spines. III. Glial sheath. Anat Embryol (Berl) 171, 245–252. [PubMed: 3985373]

Spaiardi P, Tavazzani E, Manca M, Milesi V, Russo G, Prigioni I, Marcotti W, Magistretti J & Masetto S. (2017). An allosteric gating model recapitulates the biophysical properties of $I_{K,L}$ expressed in mouse vestibular type I hair cells. J Physiol 595, 6735–6750. doi:10.1113/JP274202 [PubMed: 28862328]

Steidl JV & Yool AJ. (1999). Differential sensitivity of voltage-gated potassium channels Kv1.5 and Kv1.2 to acidic pH and molecular identification of pH sensor. Mol Pharmacol 55, 812–820. [PubMed: 10220559]

Steinacker A & Romero A. (1991). Characterization of voltage-gated and calcium-activated potassium currents in toadfish saccular hair cells. Brain Res 556, 22–32. [PubMed: 1933352]

Sun YM, Favre I, Schild L & Moczydlowski E. (1997). On the structural basis for size-selective permeation of organic cations through the voltage-gated sodium channel. Effect of alanine mutations at the DEKA locus on selectivity, inhibition by Ca^{2+} and H^{+}, and molecular sieving. J Gen Physiol 110, 693–715. [PubMed: 9382897]

Swenson RP & Armstrong CM. (1981). K channels close more slowly in the presence of external K and Rb. Nature 291, 427–429. [PubMed: 6264306]

Tucker TR & Fettiplace R. (1996). Monitoring calcium in turtle hair cells with a calcium-activated potassium channel. J Physiol 494 (Pt 3), 613–626. [PubMed: 8865061]

Ventura R & Harris KM. (1999). Three-dimensional relationships between hippocampal synapses and astrocytes. J Neurosci 19, 6897–6906. [PubMed: 10436047]

Vincent PFY, Cho S, Tertrais M, Bouleau Y, von Gersdorff H & Dulon D. (2018). Clustered Ca^{2+} Channels Are Blocked by Synaptic Vesicle Proton Release at Mammalian Auditory Ribbon Synapses. Cell Rep 25, 3451–3464 e3453. doi:10.1016/j.celrep.2018.11.072 [PubMed: 30566869]

Whim MD & Lloyd PE. (1994). Differential regulation of the release of the same peptide transmitters from individual identified motor neurons in culture. J Neurosci 14, 4244–4251. [PubMed: 8027776]

Woodhull AM. (1973). Ionic blockage of sodium channels in nerve. J Gen Physiol 61, 687–708. [PubMed: 4541078]

Zagotta WN, Hoshi T & Aldrich RW. (1990). Restoration of inactivation in mutants of Shaker potassium channels by a peptide derived from ShB. Science 250, 568–571. [PubMed: 2122520]

Zhang JF & Siegelbaum SA. (1991). Effects of external protons on single cardiac sodium channels from guinea pig ventricular myocytes. J Gen Physiol 98, 1065–1083. [PubMed: 1664454]

Zidanic M & Fuchs PA. (1995). Kinetic analysis of barium currents in chick cochlear hair cells. Biophys J 68, 1323–1336. doi:10.1016/s0006-3495(95)80305-x [PubMed: 7787021]

Zuhlke RD, Pitt GS, Deisseroth K, Tsien RW & Reuter H. (1999). Calmodulin supports both inactivation and facilitation of L-type calcium channels. Nature 399, 159–162. doi: 10.1038/20200 [PubMed: 10335846]

Key Points

- In central regions of vestibular semicircular canal epithelia, the $[K^+]_c$ in the synaptic cleft contributes to setting the hair cell and afferent membrane potentials. The potassium efflux from type I hair cells results from the interdependent gating of three conductances.
- Elevation of $[K^+]_c$ occurs through a calcium-activated potassium conductance, G_{BK}, and a low-voltage-activating delayed rectifier, $G_{K(LV)}$, that activates upon elevation of $[K^+]_c$.
- Calcium influx that enables quantal transmission also activates I_{BK}, an effect that can be blocked internally by BAPTA, and externally by a $Ca_V1.3$ antagonist or Iberiotoxin.
- Elevation of $[K^+]_c$ or chelation of $[Ca^{2+}]_c$ linearizes the $G_{K(LV)}$ steady-state I–V curve, suggesting that the outward rectification observed for $G_{K(LV)}$ may result largely from a potassium-sensitive relief of Ca^{2+}-inactivation of the channel pore selectivity filter.
- Potassium sensitivity of hair cell and afferent conductances allow three modes of transmission: quantal, ion accumulation, and resistive coupling to be multiplexed across the synapse.

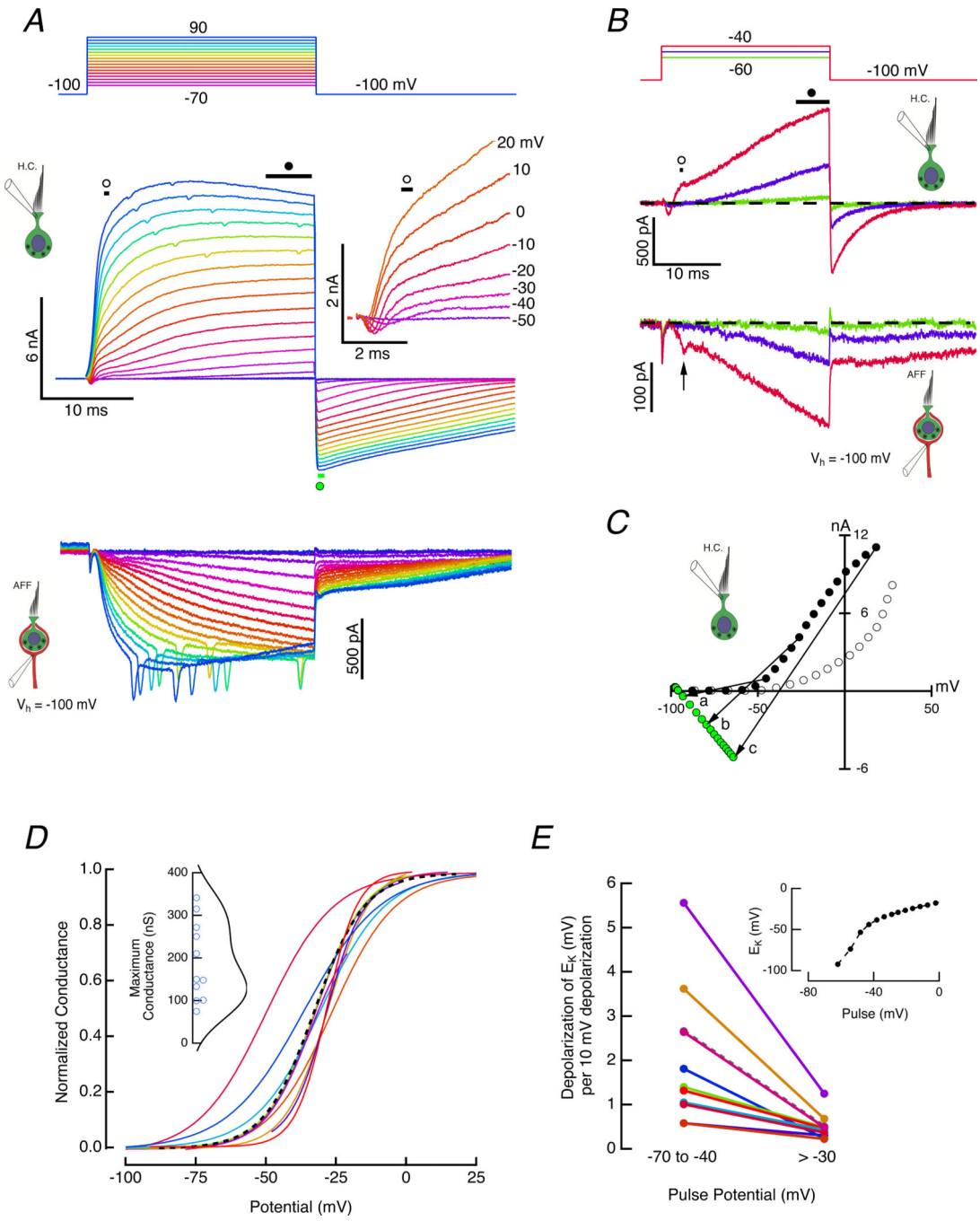

Figure 1. Dual recording of hair cell and afferent pair.

A. Both cells were clamped at −100 mV, and with the afferent potential held constant, the hair cell was depolarized for 25 ms with steps between −70 and 90 mV (top panel). Outward currents in the hair cell (middle panel) were associated with inward currents in the afferent calyx (bottom panel). Expansion of the first 5 ms revealed a rapid inward current followed by an outward current with two kinetically distinct components (middle panel, inset). Illustrated clamp potentials were corrected for the instantaneous current flow across the residual access resistance at 5 ms. *B.* Enlarged hair cell and afferent responses to hair cell

voltage commands between −60 and −40 mV. *C.* Measurement of early outward current (open circles), and final current (black, filled circles) during the step, as well as the peak tail current (green, filled circles) plotted vs voltages corrected for residual access resistance. The slope of lines connecting steady-state outward current with the peak inward current upon repolarization were used to estimate the chord conductance, and the zero-current crossing points of the lines were used to determine the instantaneous reversal potentials. The conductance (nS) and zero crossing (mV) for the three illustrated chords: a) 27.9, −78.7; b) 125.8, −58.7; c) 210.5, −37.3. *D.* Voltage-dependence of the normalized outward chord conductance for 11 hair cells. The maximum conductance ranged between 74.7 and 341.2 nS for these cells (inset). Dashed curve corresponds to cell illustrated in A. *E.* Equilibrium potential at transition *vs* potential of depolarizing step in two voltage ranges. Dashed curve corresponds to cell in A. Shift in E_K versus command potential for one cell (inset).

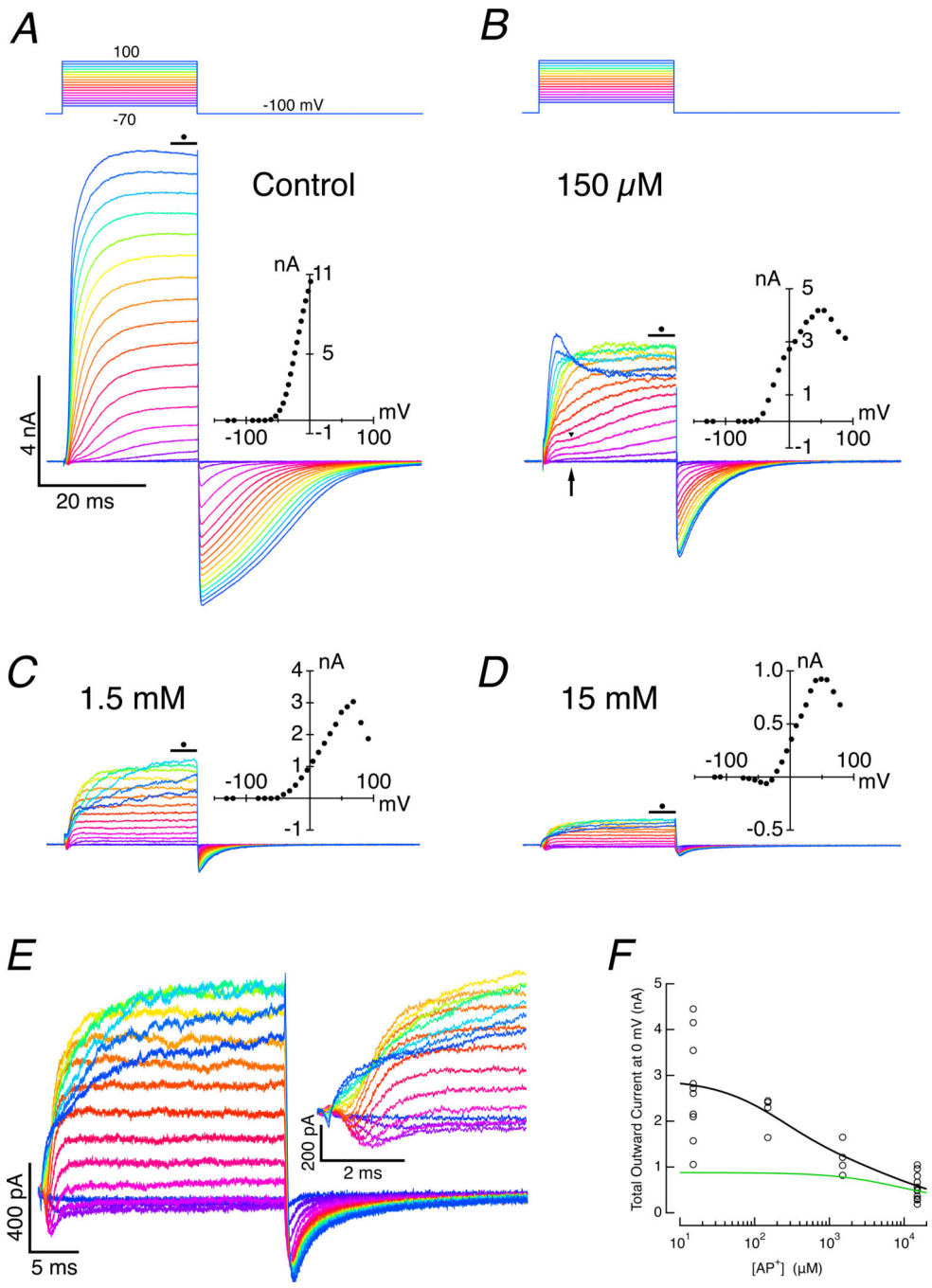

Figure 2. Dose-response of slow, outward-current block using internal 4-AP$^+$.

A. Under control conditions in the absence of 4-AP$^+$, depolarization leads to large outward currents in the hair cell. I-V curve (inset) for the last 5 ms of step was corrected for voltage drop across the residual access resistance. With large currents, hair cells failed to be depolarized much above 0 mV because of voltage drops across the residual access resistance. *B.* Hair cell response when 150 μM 4-AP$^+$ was added to the pipette solution. Maximum current was decreased, and a distinct break between the initial fast and subsequent slow components was visible (arrow). Small currents allow more depolarized

potentials to be achieved, and the N-shaped I-V curve revealed is typical of calcium-activated currents. *C.* With 1.5 mM 4-AP^+ in the pipette, the amplitude of the response in hair cells was reduced, and virtually all of the second, slow component was eliminated. *D.* The amplitude of outward current was further reduced and an early inward current was revealed when 15 mM 4-AP^+ was included in the pipette. *E.* Currents with 15 mM 4-AP^+ in the pipette on two expanded scales. *F.* Dose-response curve of outward current *vs* 4-AP^+ concentration is consistent with two currents with blocking affinities of 370 μM and 8.75 mM 4-AP^+. Two-site binding fit to total current (black), and single-site binding current for fast component alone (green).

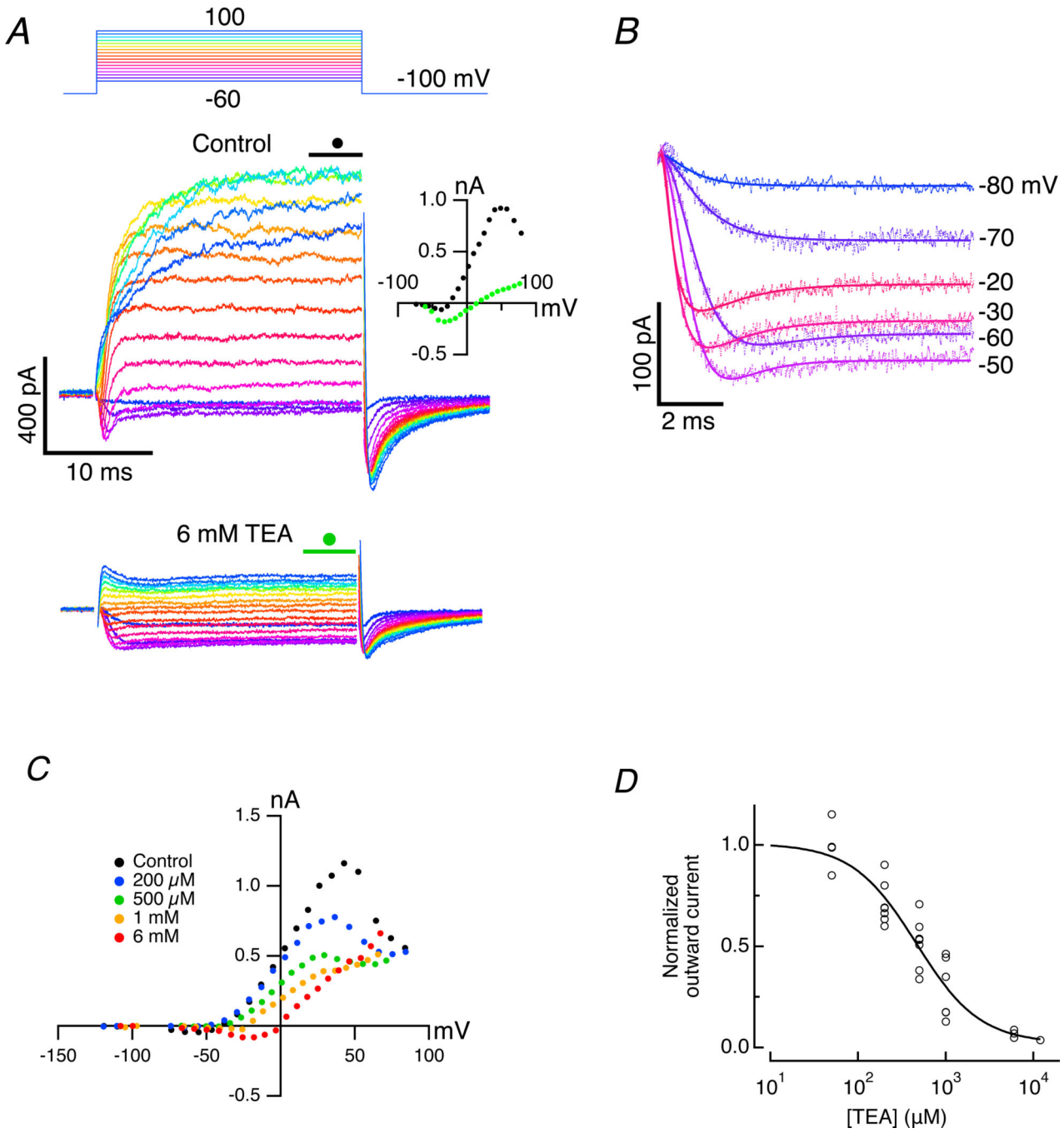

Figure 3. Block of fast outward current by TEA-Cl after eliminating slow outward current with internal 4-AP$^+$.

A. Control currents (middle panel) in artificial perilymph for command potentials between −80 and 100 mV when 15 mM 4-AP$^+$ was included in the recording pipette. Addition of 6 mM TEA-Cl blocks the fast outward current and reveals a maintained inward current for the duration of the step (bottom panel). I-V curves of the average current during final 5 ms of step (middle panel, inset) under control conditions (black filled circles), and in the presence of 6 mM TEA-Cl (green filled circles). *B.* Fits to residual inward and outward currents using Eq. 4 for command voltages between −80 and −20 mV. In the presence of 6 mM TEA-Cl,

with $n_0 = 2$ and $n_1 = 6$, the amplitude of the outward current was reduced to 9.4% of control. *C.* I-V curves for another cell using four concentrations of TEA-Cl. *D.* Normalized dose-response curve (solid line) for fits to outward current *vs* $[TEA\text{-}Cl]_o$ for multiple doses in 13 cells.

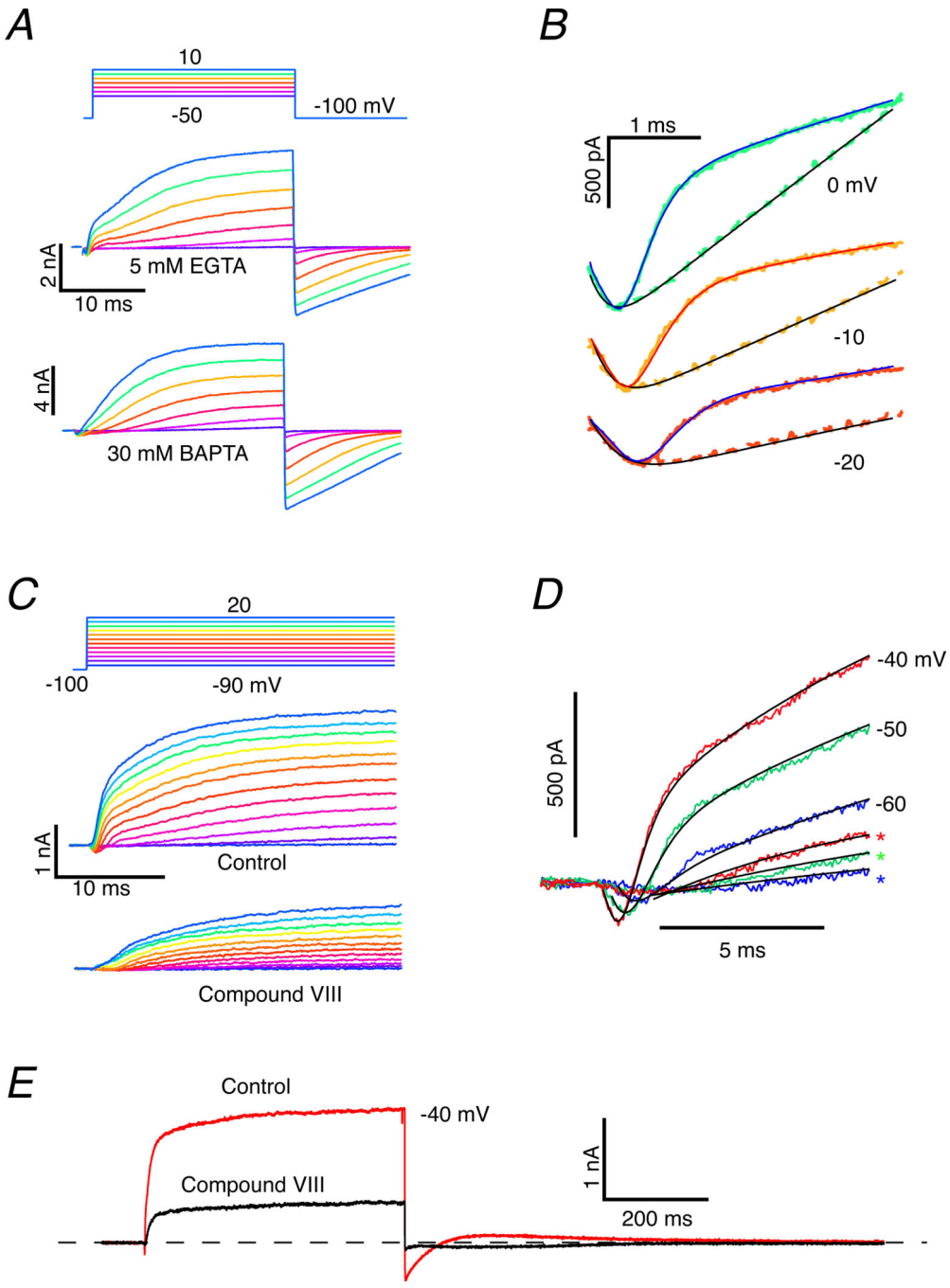

Figure 4. Increased buffering of $[Ca^{2+}]_o$, or blocking I_{Ca} blocks the rapid outward and reduces the slow outward current.

A. For voltage commands between −50 and 10 mV the current showed a rapid inward component and two outward components when internal calcium was buffered with EGTA (middle panel), but only the rapid inward and slow outward components when buffered with BAPTA. *B.* Expanded view of fits to rapid inward and slow outward currents at three voltages buffering with EGTA (solid traces) *vs* BAPTA (interrupted traces). Rapid outward current was blocked when BAPTA was used as internal buffer. *C.* Under control conditions, depolarizations elicited a rapid inward followed by rapid and slower outward currents

(middle panel). When perfused with Compound VIII, the rapid inward and outward currents were abolished and the slow outward current was reduced in amplitude. *D.* Superposition of the fits to the response under control conditions (solid lines) and with Compound VIII block (asterisks) demonstrated the effect more clearly, and revealed that the rate of rise and the saturating amplitude of the slow outward current were decreased. *E.* Currents under control conditions and in the presence of Compound VIII for the duration of a 500 ms voltage command pulse to −40 mV. Outward current was 29% of its control value in the presence of Compound VIII. Inward tail current upon repolarization was also greatly reduced.

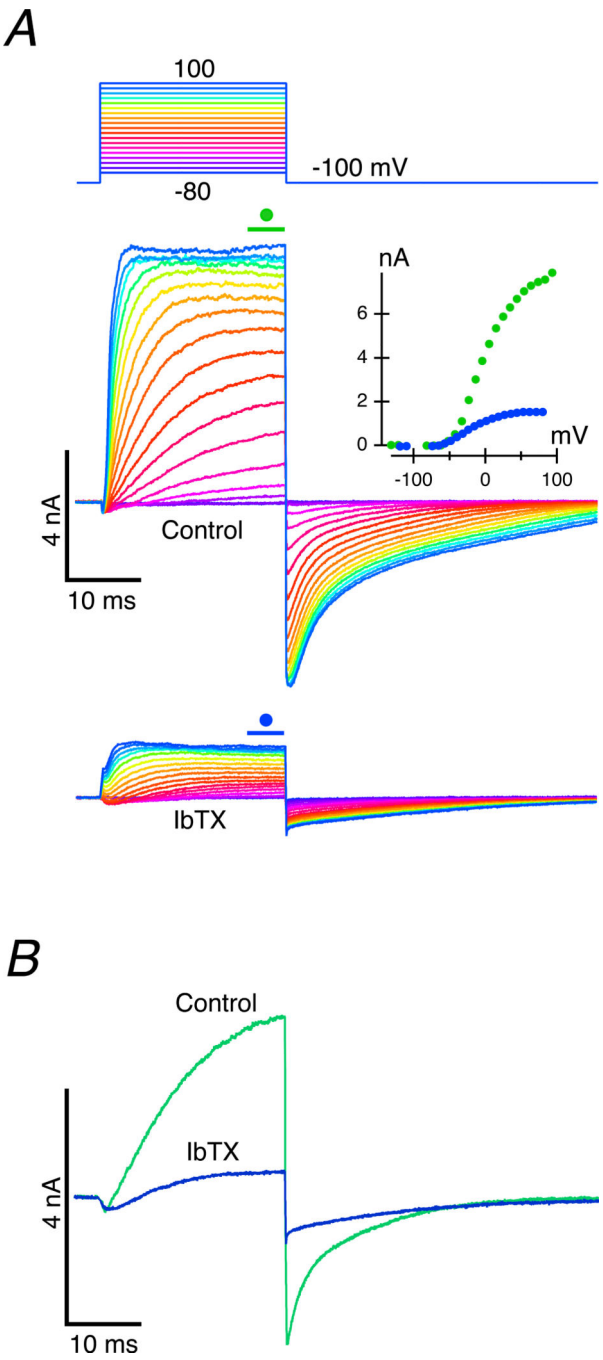

Figure 5. Iberiotoxin blocks the rapid outward potassium conductance, G_{BK}, and reduces the amplitude of the slow outward current, but leaves the rapid inward current intact.

A. Comparison of currents under control conditions (middle panel) and during perfusion of 200 nM IbTX to block the BK current (bottom panel). I-V curves for the last 5 ms of the step (inset) demonstrate reduction in the total outward current in the presence of IbTX. Measurements for hyperpolarizing voltage commands were included in the I-V. *B.* Current in response to a −10 mV command during perfusion of IbTX demonstrated a reduction to 20.2% of control.

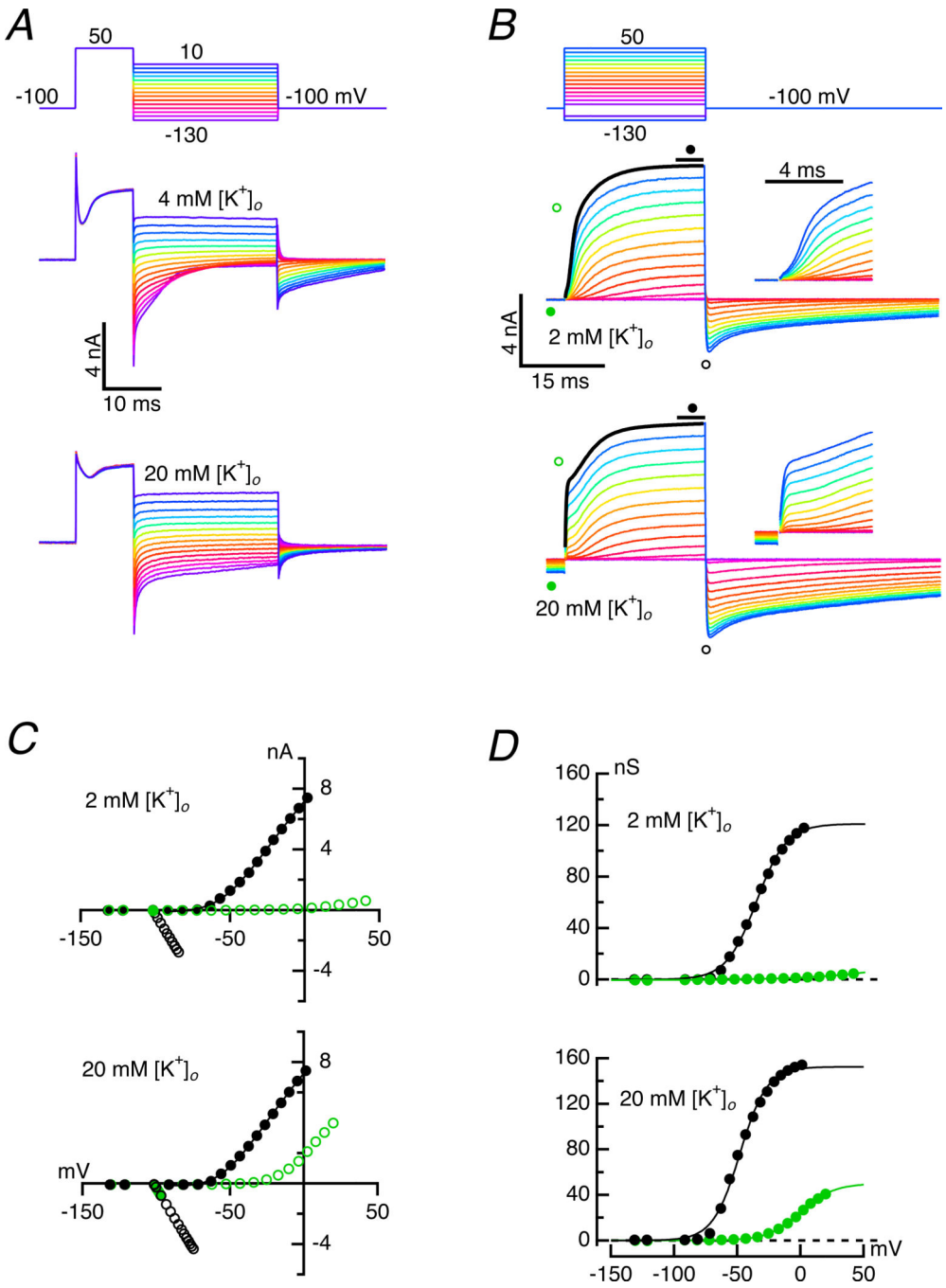

Figure 6. Effect of $[K^+]_o$ on kinetics and instantaneous current.

A. The instantaneous current in response to depolarization to 50 mV is a larger fraction of the total outward current in 20 mM (bottom panel) than in 4 mM $[K^+]_o$ (middle panel), though the total change in current was comparable. Upon repolarization to voltages between 10 and −130 mV, the inward tail current closed more rapidly and completely in 4 mM than in 20 mM $[K^+]_o$ for potentials hyperpolarized to −40 mV. *B.* Instantaneous currents for voltage series were larger in 20 mM (bottom panel) than in 2 mM $[K^+]_o$ (middle panel). Expanded views of initial 5 ms of the steps given as insets. The outward current for the

largest currents could be fit to Equation 5, to which the instantaneous current is fit by an additional first-order term with a time constant determined by the slew rate of the electrode. *C.* I-V curves of the instantaneous, or tail currents (open symbols), and steady-state current (filled circles) in 2 mM (top) and 20 mM $[K^+]_o$ (bottom). Timing of isochronal measurement indicated by corresponding symbols in B. *D.* Conductance *vs* voltage curves for the instantaneous (green open circles) and steady-state conductances (black filled circles) in 2 mM (top) and 20 mM $[K^+]_o$ (bottom).

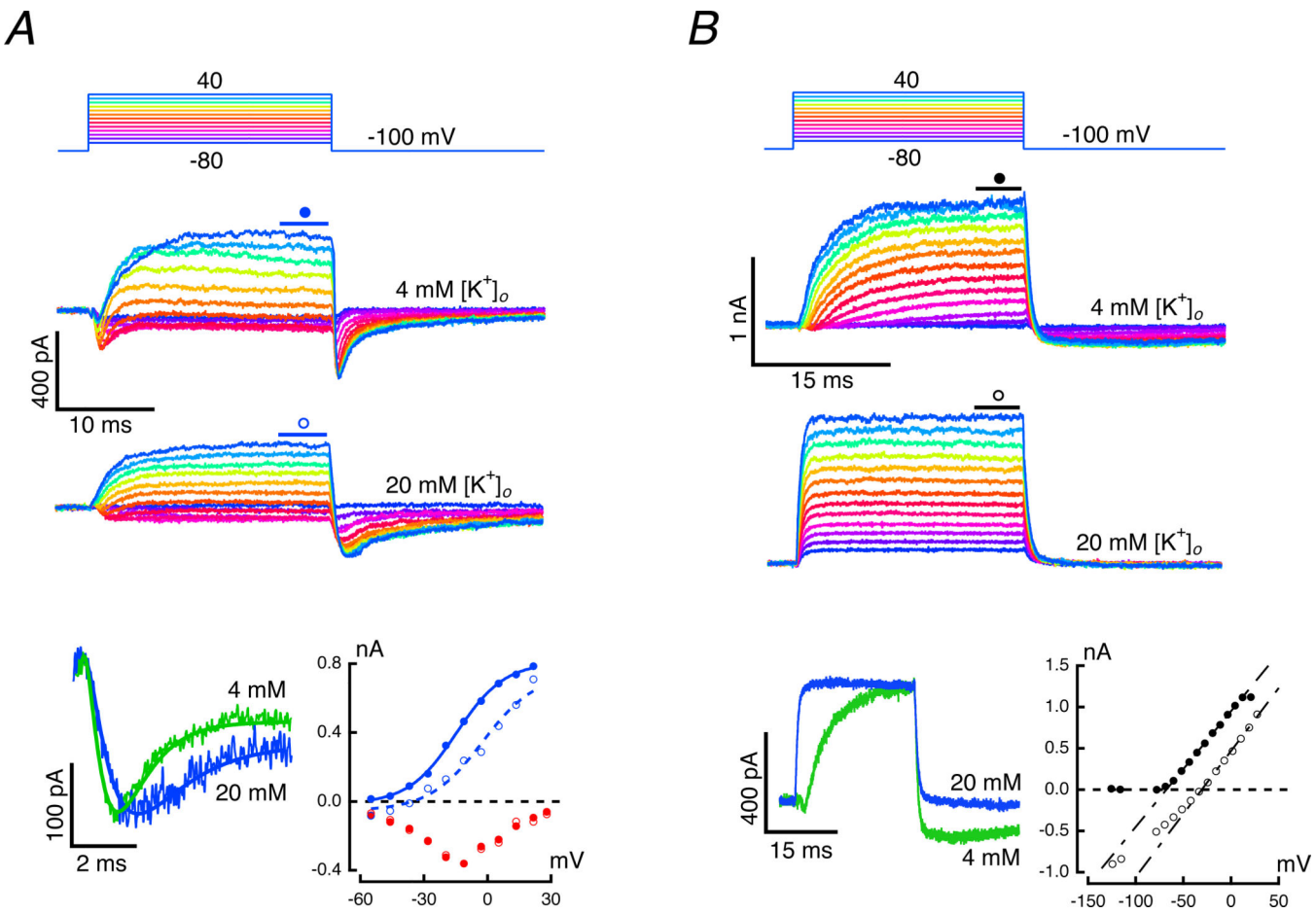

Figure 7: Potassium sensitivity of the rapid and slow outward currents.

A. Fast current in response to steps between −80 and 40 mV while perfusing 4 mM (second panel) and 20 mM $[K^+]_o$ (third panel). Superposition of responses to a −30 mV command (bottom panel, left) in 4 mM (green) and 20 mM $[K^+]_o$ (blue). Elevation of $[K^+]_o$ had no effect on the initial inward current and reduced the amplitude of the outward current. I-V curves for the fits to the inward current (bottom panel, right) in 4 mM (red filled circles) and 20 mM (red open circles), and outward current in 4 mM (blue filled circles) and 20 mM $[K^+]_o$ (blue open circles). *B.* Slow current while perfusing 4 mM (second panel) and 20 mM $[K^+]_o$ (third panel). Superposition of responses to a −30 mV command (bottom panel, left) in 4 mM (green) and 20 mM $[K^+]_o$ (blue). In the latter, the slew rate at the transitions was limited by the time constant of the recording electrode. I-V curves (bottom panel, right) in 4 mM (filled circles) and 20 mM $[K^+]_o$ (open circles). Currents for voltage commands at −130 and −120 mV (not illustrated) have been included in I-V.

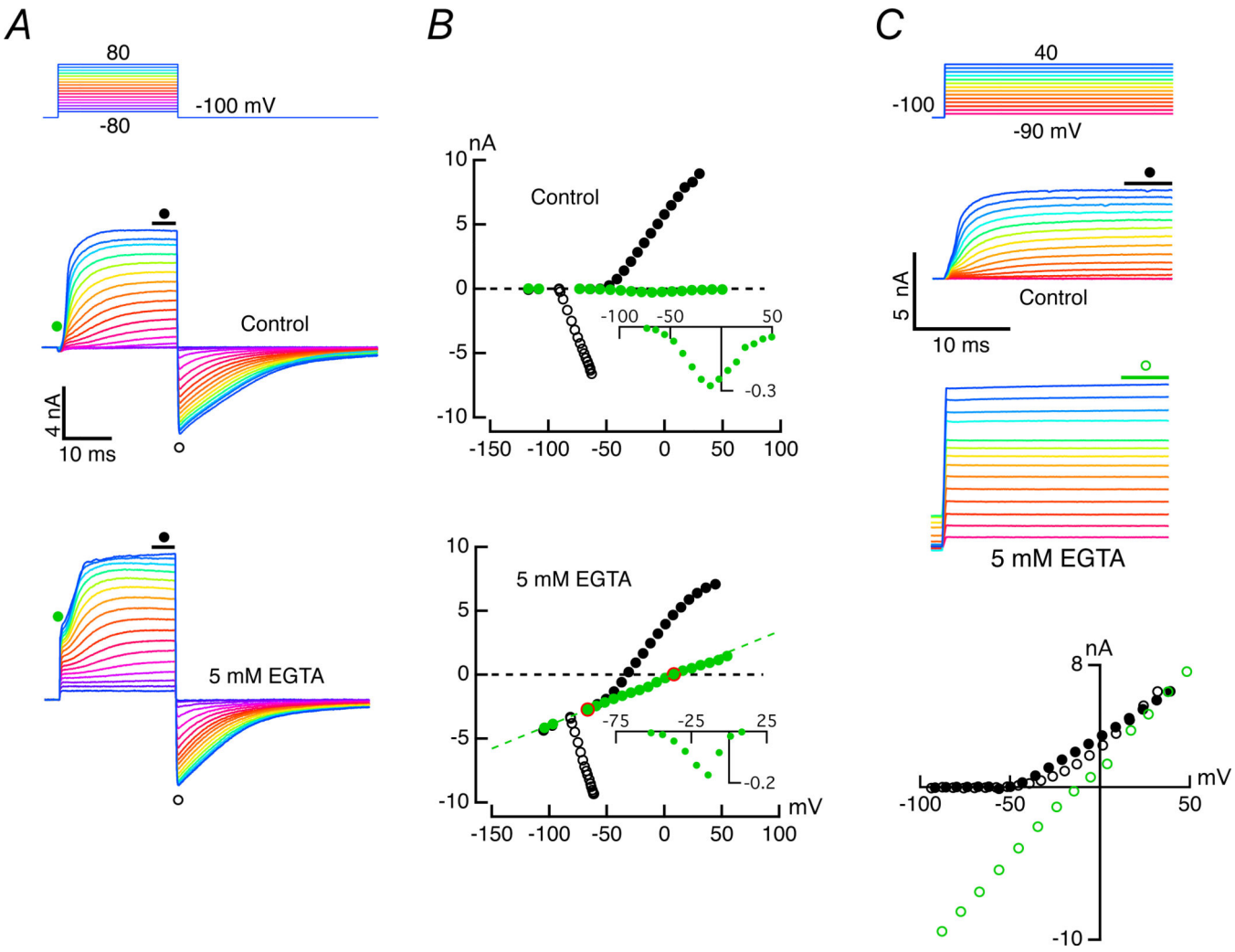

Figure 8. Effect of buffering of $[Ca^{2+}]_o$ with EGTA.

A. In contrast to the response in conventional perilymph with 2.8 mM $[Ca^{2+}]_o$ (middle panel), perfusion with perilymph containing 5 mM EGTA increased the inward holding current and the instantaneous outward current upon depolarization (bottom panel). *B.* I-V curves when perfused with 2.8 mM $[Ca^{2+}]_o$ perilymph (top) or low calcium perilymph (bottom), derived from points indicated in A. In control there was rectification with little instantaneous current. Deviation from a line fit to the leakage current (filled green circles, top) was consistent with the I-V curve for I_{Ca}. Inclusion of 5 mM EGTA reduced the outward rectification and created a leakage current across voltage (bottom). Deviation from the leak between the two red open circles was replotted as the inset. *C.* Under control conditions the rectification for the first 25 ms of 500 ms steps in 2.8 mM $[Ca^{2+}]_o$ (second panel) was linearized by inclusion of 5 mM EGTA (third panel). I-V curves for points shown in control and return control (black filled and empty circles, respectively) and in EGTA (green open circles)

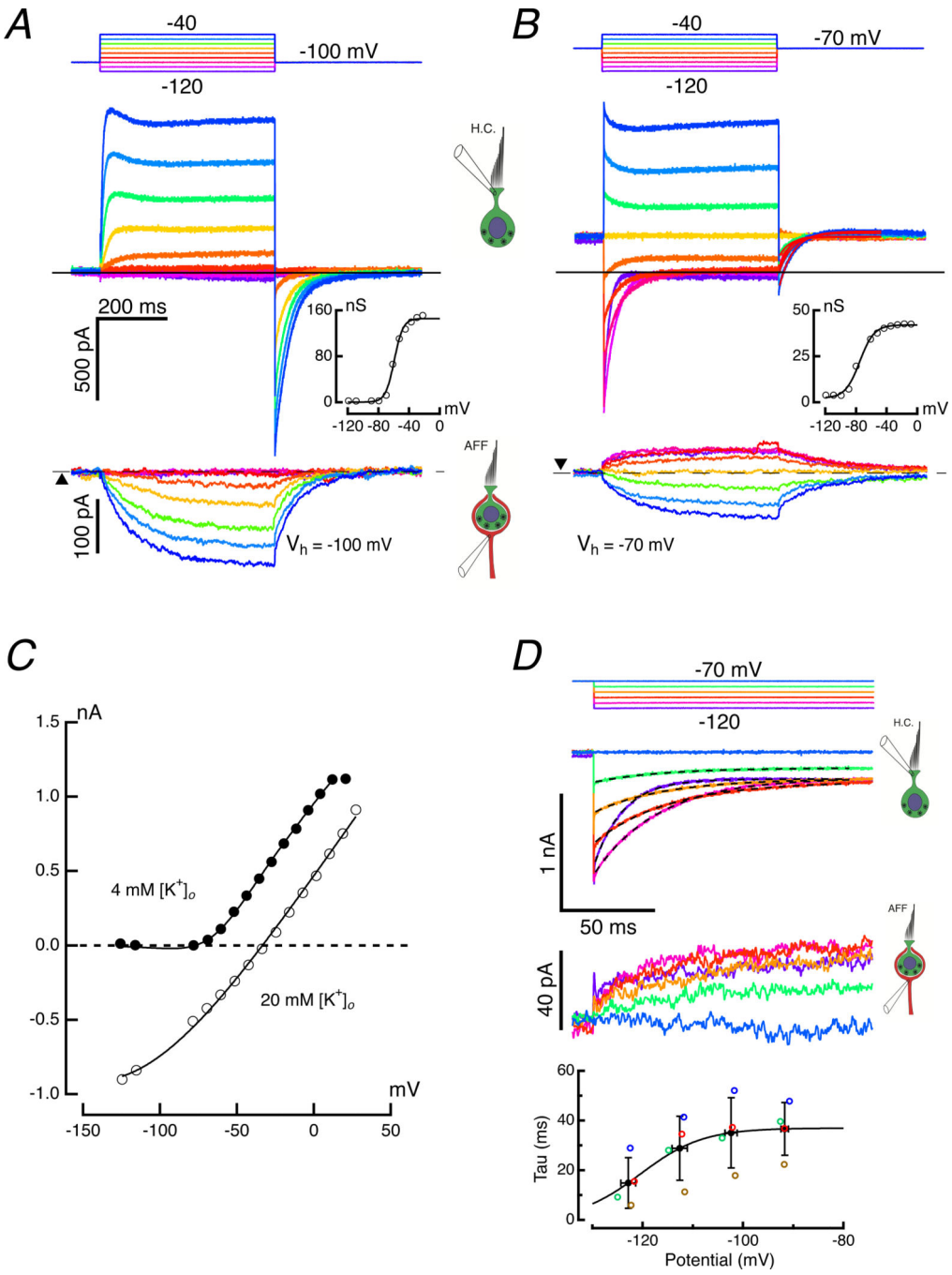

Figure 9. Voltage-dependence of hair cell current activation.

KF:KCl (10:1) internal solutions used for both hair cell and afferent. *A.* Responses in hair cell and calyx to voltage commands from a holding potential of −100 mV. Command potentials (top panel), hair cell responses (middle panel), and induced calyx response (bottom panel) over a range of voltage commands between −120 and −40 mV. The conductance *vs* voltage curve was derived from the average hair cell current during the last 5 ms of the voltage command (inset). B. Responses in hair cell and calyx to voltage commands from a holding potential of −70 mV. Response panels as in A. Compared to the

response when held at −100 mV, the smaller total conductance when held at −70 mV (inset) implies that a majority of the conductance has been inactivated at this depolarized holding potential. C. I-V curves (from Fig. 7B, bottom right) in 4 mM (filled circles) and 20 mM [K^+]$_o$ (open circles). Solid lines for each are fits to Eq. 9. *D.* Time course of deactivation of currents in hair cell (second panel) and afferent (third panel) upon hyperpolarizing hair cell from a holding potential of −70 mV. Dashed lines in second panel are single exponential fits with offset to the relaxation current. Time constants for this cell (red open circles) and three others are plotted (fourth panel). The best fit to the mean time constant (black filled circles) *vs* mean voltage (S.D. error bars shown for mean τ and voltage), assume τ was the reciprocal of the sum of the rate constants given by voltage-dependence of block in Eq. 7. Eq. 12 gave the solid line fit to τ *vs* potential with parameters: $\mu = 0.027\ M^{-1}s^{-1}$, K_B = 2.135 M, $V_B = -125$ mV, $V_e = 6.2$ mV.

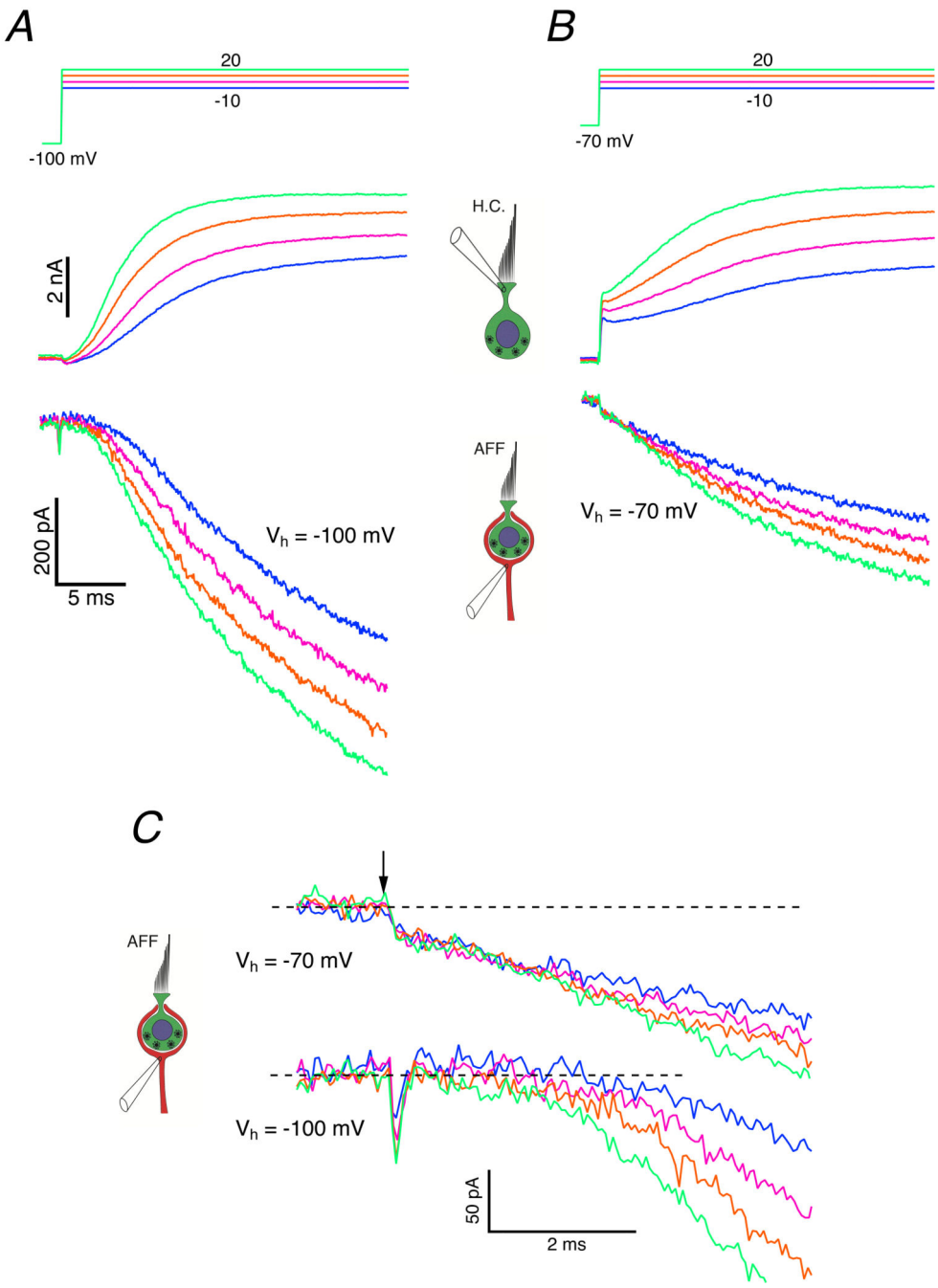

Figure 10. Hair cell and afferent response at two holding potentials.

A. Depolarizations in the hair cell produced a rapid inward current followed by a sigmodal rise in outward current (middle panel) that induced a sigmoidal increase of the inward current in the afferent (bottom panel) when both were held at −100 mV. *B.* Holding both hair cell and afferent at −70 mV yielded instantaneous outward current followed by a sigmoidal increase in the hair cell. These currents induced a nearly instantaneous jump, τ = 32 μs, in the inward current in the afferent followed by a delay, and then an exponential increase in total inward current. *C.* Expanded view of induced inward currents in the afferent. The

instantaneous outward current in the hair cell induced an inward jump (arrow), followed by an exponential increase in the afferent inward current when both were held at −70 mV. By contrast, the slow sigmoidal rise in the outward current in the hair cell induced a corresponding sigmoidal increase in the inward current when both were held at −100 mV. Voltage command steps > 90 mV imposed on the hair cell generated transient artifacts (<150 μs) in the afferent recording at the time of transition.

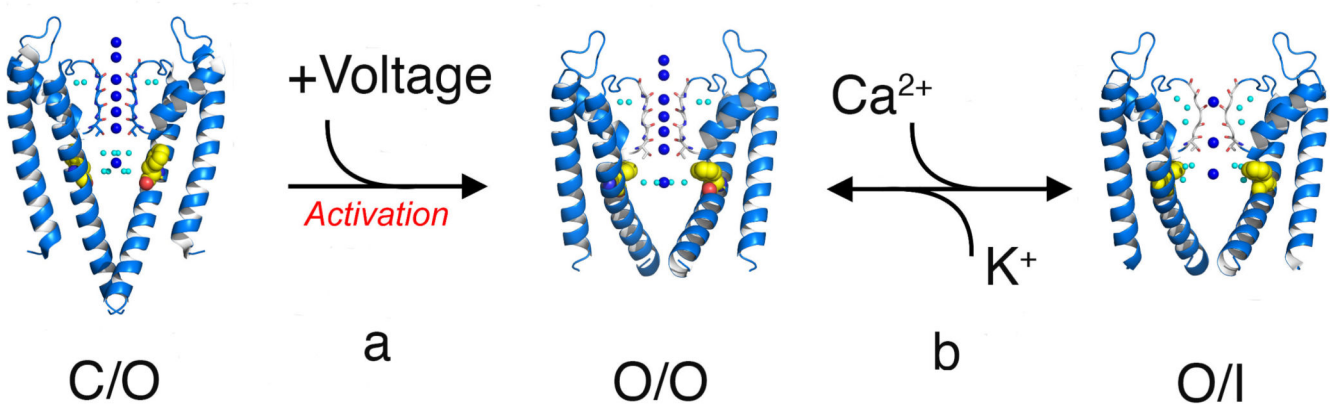

Figure 11. Sequential gating and modulation of the selectivity filter by K^+ and Ca^{2+}.

State of internal gate and selectivity given by first and second letters in diagram. Starting on the left, after recovery from inactivation at hyperpolarized potentials (C/O state), selectivity filter is open, and the internal voltage-activated gate of a channel is closed. Upon depolarization the system moves along path 'a' to the open (O/O state, middle). At depolarized potentials a fraction of the channels will transit 'b' to the inactivated state (O/I state, right). Elevation of $[Ca^{2+}]$ will move the system toward inactivation, and elevation of $[K^+]$ will move the system toward the open state. Modified with permission from Figure 8 (Cuello *et al.*, 2017), published under the Creative Commons Attribution 4.0 International Public License (CC BY 4.0; https://creativecommons.org/licenses/by/4.0).

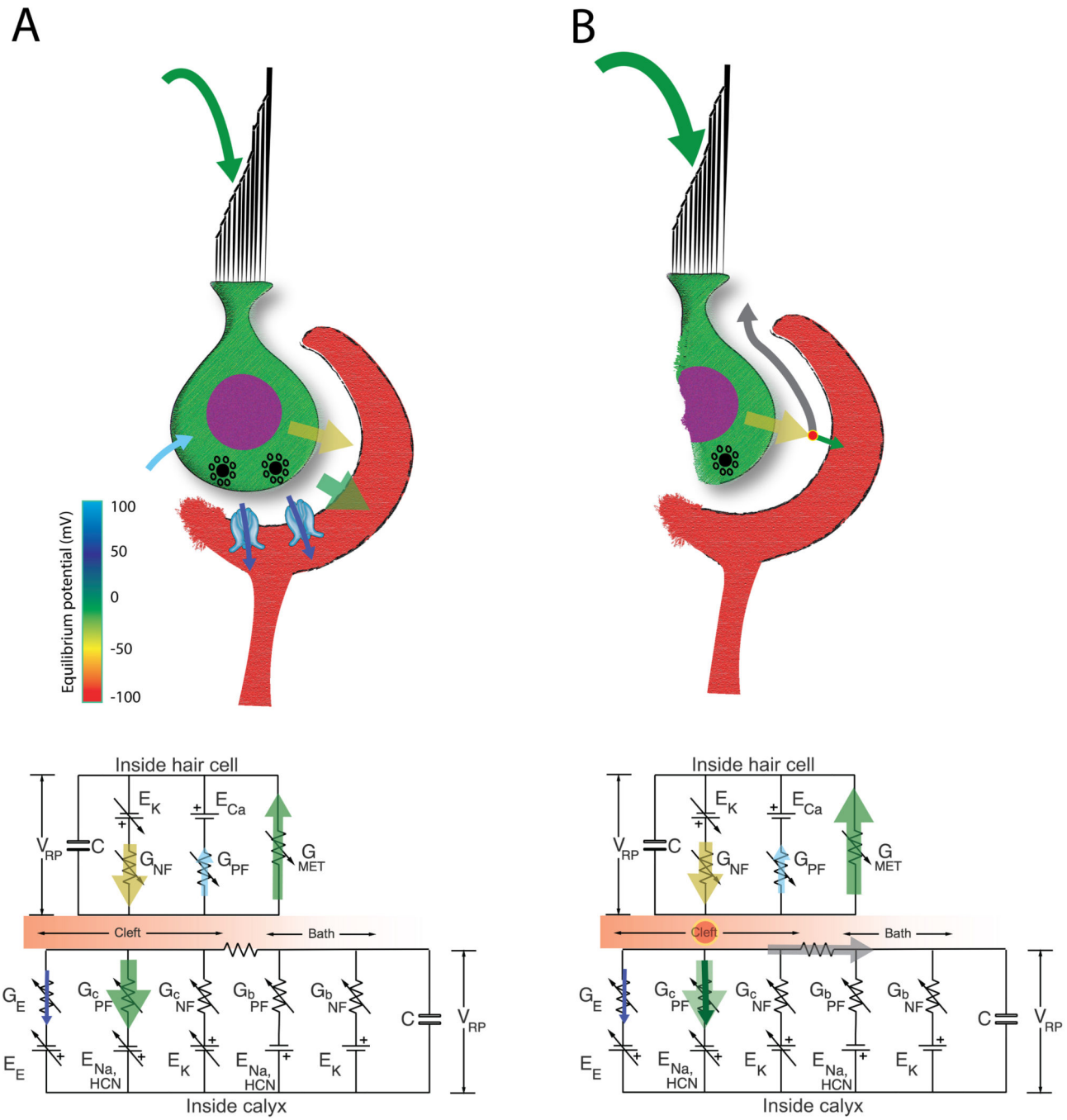

Figure 12. Three modes of synaptic transmission between hair cell and calyx afferent.

A. Synergy of synaptic cleft potassium accumulation and quantal transmission. Inward transduction current (apical green arrow) is augmented – positive feedback (PF) – by an inward I_{Ca} (light blue arrow) responsible for vesicle fusion and gating of I_{BK}. Outward potassium currents (I_{BK} and $I_{K(LV)}$) flow into the cleft (gold arrow) – negative feedback (NF) – and increase $[K^+]_c$. This elevation increases the $G_{K(LV)}$, but decreases the driving force through the NF components, with the result that the hair cell depolarizes to a potential where inward and outward currents balance. On the inner face of the calyx, the elevation in

$[K^+]_c$ increases the HCN conductance, G_{cPF}, and a mixed Na^+ and K^+ current depolarizes the calyx (large green arrow). Ion accumulation in the cleft brings cells to potentials where calcium influx causes the fusion of synaptic vesicles in the hair cell, and brings the calyx afferent to potentials within a few mV of the threshold for generation of action potentials. Glutamate released from hair cell gates inward current (dark blue arrows) through the calyx AMPAR. *B*. Dynamic resistive coupling in the absence of gap junctions is produced by hair cell $G_{K(LV)}$ and calyx $G_{cPF(HCN)}$ on at the resting potentials on the inner face of the calyx. As G_{HCN} increases, an increased fraction of the current flowing out of the hair cell is diverted to flow into the calyx afferent (dark green arrow), rather than through the synaptic cleft (grey arrow) out into the bath. A second limb of G_{bPF} is included to represent HCN channels on the outer face of the calyx.